Journal of Building Engineering 98 (2024) 111480

Contents lists available at ScienceDirect

Journal of Building Engineering

journal homepage: www.elsevier.com/locate/jobe

Reliability and sustainability integrated design optimization for engineering structures with active machine learning technique

Enyong Zhao [a], Qihan Wang [a,b,**], Mehrisadat Makki Alamdari [a], Zhen Luo [b], Wei Gao [a,*]

[a] Centre for Infrastructure Engineering and Safety, School of Civil and Environmental Engineering, The University of New South Wales, Sydney, NSW, 2052, Australia

[b] School of Mechanical and Mechatronic Engineering, The University of Technology Sydney, Sydney, NSW, 2007, Australia

ARTICLE INFO

Keywords:
Reliability and sustainability integrated design optimization
Uncertainty quantification
Embodied carbon
Active learning
Machine learning technique

ABSTRACT

Recent strategic plans from many governments share the same emphasis on sustainable development goals. The construction industry is recognized as one of the primary contributors to greenhouse gas emissions. Stimulated by such political and practical requirements, this research aims to develop a reliability and sustainability integrated design optimization (RSIDO) framework for engineering structures. Statistical modelling is conducted which provides probabilistic models for embodied carbon coefficients (ECCs). The proposed RSIDO framework contains three main stages. The first stage solves the classical reliability-based design optimization (RBDO) problem. The second stage conducts the reliability-based embodied carbon quantification to define the sustainable reliability constraint. Lastly, the new sustainable probabilistic design constraint is embedded in the design question. Furthermore, to overcome the computational difficulty, an active-learning extended-support vector regression (AL-X-SVR) technique is proposed to improve the computational efficiency of the proposed framework. The embedded regression algorithm is presented with consolidated theoretical backgrounds. Further, an active learning strategy is implemented to select the learning samples efficiently. The applicability and effectiveness of the proposed AL-X-SVR method are demonstrated using a highly nonlinear-constrained mathematical validation. Additionally, the RSIDO framework is demonstrated through three engineering applications. This research contributes a comprehensive framework that not only addresses reliability and sustainability but also enhances computational efficiency, thereby introducing an innovative approach to design optimization in building engineering.

1. Introduction

As global warming continues to pose new challenges, sustainable engineering strategies are receiving increasing attention. Buildings are found to be responsible for up to 39 % of the total embodied carbon globally [1]. Furthermore, the total global embodied energy is expected to keep escalating due to a wide range of social activities. The total carbon emission for a building involves the

* Corresponding author.
** Corresponding author. Centre for Infrastructure Engineering and Safety, School of Civil and Environmental Engineering, The University of New South Wales, Sydney, NSW, 2052, Australia.
E-mail addresses: qihan.wang@unsw.edu.au (Q. Wang), w.gao@unsw.edu.au (W. Gao).

https://doi.org/10.1016/j.jobe.2024.111480
Received 13 August 2024; Received in revised form 27 October 2024; Accepted 1 December 2024
Available online 2 December 2024

construction stage and operation stage. Pomponi and Moncaster [2] point out that the operation-induced carbon emission has reduced and the transformation to zero-energy buildings is in progress. Therefore, embodied carbon during the construction stage should be more of a focus. According to the United Nations Environmental Programme, the embodied carbon induced by the construction sector alone is 10 % of the total greenhouse gas emissions worldwide [3]. H.L. Gauch et al. [4] state that the embodied carbon is not only increasing in comparison to the operational carbon but also in absolute terms. From an engineering perspective, the decision-making process to design structures considering embodied carbon involves two main problems, the quantification of embodied carbon and design optimization [5].

Despite the growing attention on embodied carbon quantification, current methodologies either lack comprehensive uncertainty quantification approaches or fail to integrate structural reliability with sustainability considerations. Moreover, the life cycle assessments and reliability-based design optimization (RBDO) have been explored in previous studies, but there is still a notable gap in addressing how embodied carbon can be effectively controlled within a reliability-based framework that simultaneously considers environmental impact and structural performance. Hence, no well-established framework to simultaneously integrate RBDO and the concept of sustainability can be found in the literature.

This study proposes a reliability and sustainability integrated design optimization (RSIDO) framework to incorporate the concept of both embodied carbon and structural reliability in design practice. The framework consists of three stages. Stage I involves the original RBDO problem. Stage II is reliability-based embodied carbon uncertainty quantification and selection of the embodied carbon reduction strategy. Lastly, the embodied carbon threshold calculated in the previous step is implemented to form an RBDO problem as Stage III. The challenges in embodied carbon quantification and design optimization are presented next.

Regarding embodied carbon quantification, recent relevant literature is reviewed. The embodied carbon of buildings needs to be determined by different factors such as building designs, construction methods, transportation distance, human errors. This can potentially cause the final embodied carbon to exceed the intended volume. Quantification and control of the embodied carbon during construction are undoubtedly becoming important under these uncertainties. To quantify the Embodied Carbon of engineering structures, the life cycle assessment (LCA) method has been used by many practitioners [6–10]. Pan and Teng [1] systematically assessed the impact of different methodological variables on embodied carbon. The authors obtain a more comprehensive understanding of the embodied carbon assessment process by analysing eleven variables from temporal differences, spatial disparities, procedural inconsistencies, and physical diversities. It is stated that the embodied carbon assessment provides a large variation realistically. Li et al. [11] identified the uncertainties in the LCA of buildings and their finding was that some least-influential sources of uncertainties suggested by previous studies are the most-influential. This conflict between various researchers further highlights the lack of standardization of the embodied carbon quantification process. As abovementioned, the quantification process for embodied carbon is likely to confront difficulties due to the lack of sufficient statistics to systematically describe the embodied carbon coefficient for common construction materials. Thus, uncertainty quantification and RBDO cannot be conducted effectively. To generate a credible statistical model to represent embodied carbon coefficients, this paper first reviews and compiles existing studies to establish statistical models of the embodied carbon coefficients for two common construction materials: concrete and steel. Based on these statistical models, a probabilistic uncertainty quantification of embodied carbon for engineering structures made from these materials can be achieved. The probabilistic uncertainty quantification incorporates reliability analysis, where the reliability index indicates the likelihood that the embodied carbon remains below a set threshold, accounting for uncertainties in embodied carbon coefficients of material. This process is applied to evaluate the embodied carbon reliability, which will later support a reliability-based design optimization process aimed at designing within specified reliability thresholds.

As for design optimization, it is known that structural performance is often affected by inherent uncertainties including geometrical and material imperfection, loading conditions, and environments. As a result, it is crucial to take a probabilistic approach to analyze and optimize the structure to ensure its integrity and eliminate failures. Therefore, in the design optimization part, reliability-based design optimization (RBDO) is used to solve for the optimal design that satisfies the reliability constraint. Different RBDO methods have been proposed in the past. The two-level method contains two loops, where the outer loop optimizes for the design objectives, and the inner loop checks if the probability constraints are satisfied. Structural reliability analysis methods are used for the inner loop. The Monte Carlo Simulation (MCS) is the most straightforward approach that calculates the probability of failure by simulating a large number of structural responses. In practice, the limit state functions are often implicit and time-consuming. Eventually, the MCS will be operationally infeasible. Methods such as the first-order reliability method (FORM) and second-order reliability method (SORM) utilize the definition of the most probable point (MPP) to approximate the reliability index with the first and second-order Taylor expansion [12]. Based on the MPP, the Reliability Index Approach (RIA) and Performance Measure Approach (PMA) were proposed [13]. Besides the two-level methods, the single-loop approach (SLA) and decoupled approaches have also been studied [14,15]. The SLA reformulates the RBDO problem by moving the probabilistic constraints into the deterministic optimization using optimality conditions. The decoupled approach, Sequential Optimization and Reliability Assessment (SORA) [16] separates the optimization and reliability analysis into cycles of deterministic optimization and reliability analysis. However, these MPP-based methods can reduce the computational costs for engineering applications but would introduce inaccuracy for highly nonlinear limit state functions. Further, the heavy computational cost is still the biggest challenge for practical applications.

To alleviate the abovementioned problems, the surrogate-based structural reliability analysis and RBDO have been investigated extensively in the last decade. Some popular surrogate models include artificial neural networks (ANN) [17–19], Kriging [20,21], polynomial chaos expansion (PCE) [22,23], random forest (RF) [24,25] and support vector regression (SVR) [26–28]. Although all these surrogate models are capable of approximating the relationship between the structural inputs and the structural response using far fewer data points compared to the MCS, computational costs are still being wasted on some uninterested regions of the performance function as the structural reliability analysis only requires the accuracy of the limit state boundary. Some adaptive sampling techniques

have been developed to increase computational efficiency further. The fundamental idea is to adaptively select samples that would generate the surrogate model with the highest accuracy around the limit state function. Many different learning functions have been proposed including, the U-function [21], expected feasibility function (EFF) [29], least improvement function (LIF) [30], and REIF [31]. Zhang et al. [32] proposed the use of double-loop Kriging to approximate the reliability index function (RIF) which constructs the surrogate model between the design inputs and reliability index directly, and the RBDO can then be transferred into a deterministic optimization problem. On the other hand, the SVR is known for its capability for high-dimensional problems.

This study proposes a novel Active-Learning Extended Support Vector Regression (X-SVR)-assisted structural reliability analysis strategy to serve as the inner loop of the RBDO problem, namely Active-Learning X-SVR-assisted (AL-X-SVR) for RBDO. The X-SVR is implemented as the surrogate modelling technique due to its multiple successes in structural reliability analysis including a wide range of engineering applications including static, elastoplastic, dynamic, and polymorphic scenarios [33–35]. The problem of X-SVR can be formulated as a convex optimization problem, specifically a Quadratic Programming (QP) problem. It means that the global optimal solution can be achieved through any QP or convex solver. This feature of convexity theoretically supports the accuracy of the surrogate model established by the X-SVR algorithm. Further, the proposed method implements the two-level RBDO approach while conducting a double-loop global-local two-stage enrichment process to maximize the sampling efficiency. Overall, the proposed method takes advantage of both the X-SVR technique and the active-learning strategy which improves the model accuracy and convergence speed. This ensures that the computational cost waste on unnecessary sample points of the optimization process can be eliminated.

The proposed RSIDO framework provides a new perspective in design methodology by integrating the aspects of embodied carbon and structural reliability. The framework is structured into three stages, each contributing to the entire sustainable design process. In Stage I of the RSIDO, the traditional RBDO problem is solved. The proposed AL-X-SVR technique is adopted herein to increase the computational efficiency by approximating the complex, and computationally expensive simulations. The active learning module ensures that the new samples are added towards the critical region of the design space, iteratively improving the accuracy without the need to evaluate the original limit state function for space-filling samples. Stage II introduces the probabilistic uncertainty quantification of embodied carbon and new embodied carbon constraint. By quantifying the embodied carbon within the reliability framework, the RSIDO allows the design to understand the environmental impact of the primary design solution. In Stage III, the new embodied carbon threshold calculated in the previous step is incorporated back into the RBDO problem. This implements an additional reliability constraint which is subjected to the quantity of embodied carbon caused by the structure. This ensures the final design adheres to the embodied carbon limit while satisfying the structural reliability requirement. Once again, the AL-X-SVR-assisted RBDO is adopted for this design problem. The previously constructed surrogate model in Stage I is still employed. The optimal region is likely to shift due to the impact of the new design constraint. However, the latest surrogate is still capable of predicting the response of the limit state surface due to the earlier global enrichment process. The use of the AL-X-SVR is a key innovation of the proposed method, which improves computational efficiency by focusing on optimal regions in the design space. This adaptive strategy reduces computational cost while maintaining high accuracy, even when the design space shifts due to new constraints, such as those imposed by embodied carbon threshold. The X-SVR's capability to formulate the surrogate model construction process as a convex QP optimization problem, ensures the optimal solution can be achieved. Furthermore, overfitting can be avoided by hyperparameter autotuning which is supported using Bayesian optimization and cross-validation. The active learning feature is implemented to further boost the efficiency of the surrogate modelling. Overall, the RSIDO framework provides a path for designers to design reliable structures more sustainably. The reliability-based approach for both structural performance and embodied carbon quantity aligns with the current design approach.

The remainder of this paper is structured as follows. In Section 2, the RBDO problem is briefly reviewed and the currently available inventories for embodied carbon coefficients are reviewed and analysed. The proposed RSIDO framework is introduced. In Section 3, The RBDO and X-SVR formulations are introduced in Section 3. In Section 4, the detailed proposed framework of AL-X-SVR-assisted RBDO with embodied carbon is presented. In Section 5, a highly nonlinear constraint RBDO test function is investigated to validate the applicability of the proposed method. In Section 6, three engineering applications have been investigated to further demonstrate the effectiveness and computational efficiency of the proposed framework. The conclusions are drawn in Section 7.

2. Reliability and sustainability integrated design optimization

2.1. Traditional reliability-based design optimization

The traditional reliability-based design optimization (RBDO) is defined as an optimization problem with an objective and subjected to probabilistic constraints, i.e.,

$$\begin{aligned} &\text{Find } \mathbf{d}^{*} \text{ for } \min f(\mathbf{X},\mathbf{d}) \\ &s.t. \quad \Pr[g_i(\mathbf{X},\mathbf{d}) \le 0] \le \Phi\left(-\beta_{\text{target},i}\right) \ \text{ for } i = 1,\ldots,n \\ &\mathbf{d}_l \le \mathbf{d} \le \mathbf{d}_u \end{aligned} \tag{1}$$

where the $f(\mathbf{X},\mathbf{d})$ denotes the objective function of the RBDO problem and the $g_i(\mathbf{X},\mathbf{d})$ denotes the i-th limit state function. The $\mathbf{X} \in \Re^{n_R}$ and $\mathbf{d} \in \Re^{n_d}$. denote the random variable and design variables, which n_R and n_d denote the dimensions of design variables and random variables, respectively. $\beta_{\text{target},i} \in \Re$ denotes the target reliability index for i-th failure mode, and the design variable boundaries are defined as $[\mathbf{d}_l, \mathbf{d}_u]$. The $\Pr\left[g_i(\mathbf{X}) \le 0\right]$ denotes the probability of failure of the i-th failure mode, which can be written as a multi-

dimensional integration problem,

$$P_f = \Pr[g_i(\mathbf{X}, \mathbf{d}) \leq 0] = \int \cdots \int_{g_i(\mathbf{X},\mathbf{d})<0} f_{\mathbf{X}}(\mathbf{X}, \mathbf{d})\, \mathrm{d}\mathbf{X} \tag{2}$$

where the $f_{\mathbf{X}}(\mathbf{X}, \mathbf{d})$ denotes the joint probability density function (PDF) of $\mathbf{X}$.

Solving this multi-integration expression analytically is extremely challenging. The Monte Carlo Simulation (MCS) method is the most straightforward manner to handle this problem, but it requires tremendous iterations to achieve credible estimations. This may lead the problem to be computationally infeasible, especially when a single computation of the limit state function has already been time-consuming. Initially, approximation methods such as FORM and SORM are developed to reduce the number of function evaluations required. As well as variance-reduction techniques to improve the efficiency of MCS. These two approaches still demand heavy computational costs as reliability analysis is required for every optimization iteration.

In the past, various RBDO algorithms have been proposed including the surrogate-assisted method [20,32,36]. Adaptive sampling or active learning strategies are gaining increasing popularity as they only sample important regions while being able to provide accurate surrogate models for the original problem [21,37–39]. In this research, the Active-Learning Extended-support vector regression-assisted (AL-X-SVR) is proposed for the RSIDO problem. To achieve a sustainable design solution while satisfying the reliability constraints, the limit state function needs to be evaluated excessive times. For engineering structures with implicit limit state function, this process is very computationally heavy. Therefore, the Extended-support vector regression (X-SVR) is selected as the surrogate modelling technique, and it is integrated with an active learning strategy to enhance the efficiency of the X-SVR.

2.2. Statistical modelling for embodied carbon coefficient

The study of embodied carbon evaluation in the built environment has swiftly expanded as a research subject, driven by the significance of the matter in connection to climate concerns. In this section, the up-to-date data inventory and relevant publications for embodied carbon of common construction materials have been reviewed. It was discovered that even for the same type of material in the same grade, uncertainty still exists in their embodied carbon coefficients (ECC). From the literature, the underlying cause is manifold. Pan and Teng [1] investigated this variability of embodied carbon emission of buildings from temporal, spatial, procedural, to physical. This study from 244 cases has revealed that not all assessments have been conducted completed and transparently defined, which builds up the barrier for estimating and quantifying the EC in structures. Wu, Feng [40] suggest that selecting an appropriate ECC is challenging for someone lacking expertise and can be a time-consuming process. Overall, this decision-making can be correlated to different perspectives of decision-makers. Therefore, a comprehensive analysis of statistical modelling for the ECC of common construction materials is essential.

To establish relatively credible statistical models of the ECC, the cradle-to-gate stages including raw material extraction, transportation and manufacturing are taken into account for steel and concrete. The ECCs of the two most common materials in modern construction, concrete and steel have been retrieved from the database and publications [41–65] and are summarized in Table 1. The ECCs are expressed in kg of CO_2 per kg of material, i.e., $kgCO_2/kg$.

The established database contains 120 sets of data for concrete and 197 sets for steel, respectively. The statistical information of their ECCs is depicted in Fig. 1.

From Fig. 1, it can be noticed that the ECC inherently with large variations for both types of materials: ranging from 0.033 to 0.9 $kgCO_2/kg$ for concrete; and 0.282 to 16.155 $kgCO_2/kg$ for steel. To achieve a considerate estimation of total embodied carbon in engineering, it is significant to introduce the concept of uncertainty quantification and establish relatively appropriate statistical models. Herein, the maximum likelihood estimation method (MLE) is adopted to conduct the statistical modelling of the ECCs for both concrete and steel.

A series of distribution types, including Normal, Lognormal, Gumbel, Weibull, and Gamma distributions, are used for hypothesis testing. The fitted distributions for concrete and steel are depicted in Figs. 2 and 3, respectively, with quantile-quantile (q-q) subplots. The q-q plots present the quantiles of the sample data versus the theoretical quantile values from a specific distribution. If the sample data follows the theoretical distribution, the points should align along a straight line. It is often used to estimate the fitting performance by providing a graph that indicates goodness of fit.

In Figs. 2 and 3, the histograms of ECCs for concrete and steel are plotted as well as the fitted distribution curves of the selected distribution types. It is evident that none of the eight distribution fittings perfectly match the collected data. This is expected due to the significant variability of data points and the limited amount of data. However, the most representable distribution-fitting results are selected for each construction material. The q-q plots of all distribution fittings are analysed based on the Root Mean Square Errors (*RMSE*),

Table 1
Number of collected datasets and their statistical features (Unit: $kgCO_2/kg$).

Material	Available datasets	Covering stages	Minimum	Maximum	Mean
Concrete	120 sets	Cradle-to-gate	0.033	0.9005	2.2585
Steel	197 sets	Cradle-to-gate	0.282	16.155	0.1649

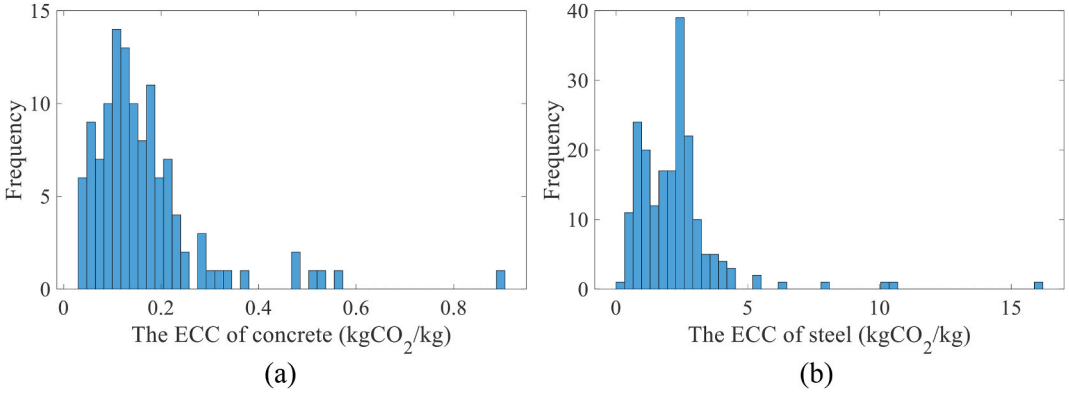

Fig. 1. The published data for (a) ECC of concrete and (b) ECC of steel [2,66–70].

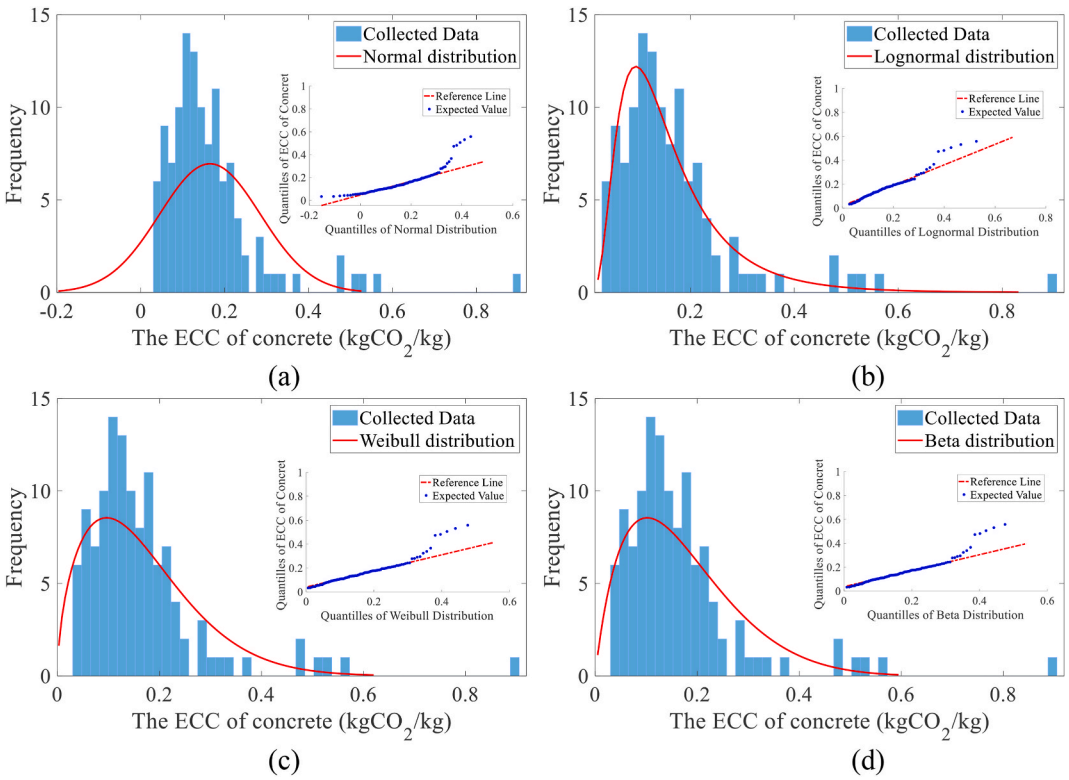

Fig. 2. The distribution fitting for the collected data of ECC of concrete against (a) Normal distribution, (b) Lognormal distribution, (c) Weibull distribution, and (d) Beta distribution.

$$RMSE = \sqrt{\frac{1}{n}\sum_{i=1}^{n} d_i^2} \tag{3}$$

where the $d_i = \left|Q_{Theoretical,i} - Q_{Collected,i}\right|$ denotes the absolute difference as a discrepancy measurement. The *RMSE* values are calculated and presented in Table 2.

Based on the *RMSE* of the q-q plot for concrete and steel, it can be found that the Lognormal distribution mostly describes the ECC distribution of concrete, and the Gamma distribution describes the ECC distribution of steel the best. Through hypothesis testing, the ECCs of concrete and steel are fitted as $\psi_{\text{concrete}} \sim Lognormal\left(-1.9903, 0.5993^2\right)$ and $\psi_{\text{steel}} \sim Gamma(2.8155, 0.05855)$, respectively, in the unit of $kgCO_2/kg$, where $Lognormal\left(\mu, \sigma^2\right)$ denotes the lognormal distribution with the location parameter μ and scale parameter σ, and $Gamma(\alpha, \beta)$ denotes the Gamma distribution with the shape parameter α and rate parameter β. While it is observed that the differences between the various ECC distributions may not be statistically significant, the selected distributions demonstrate better

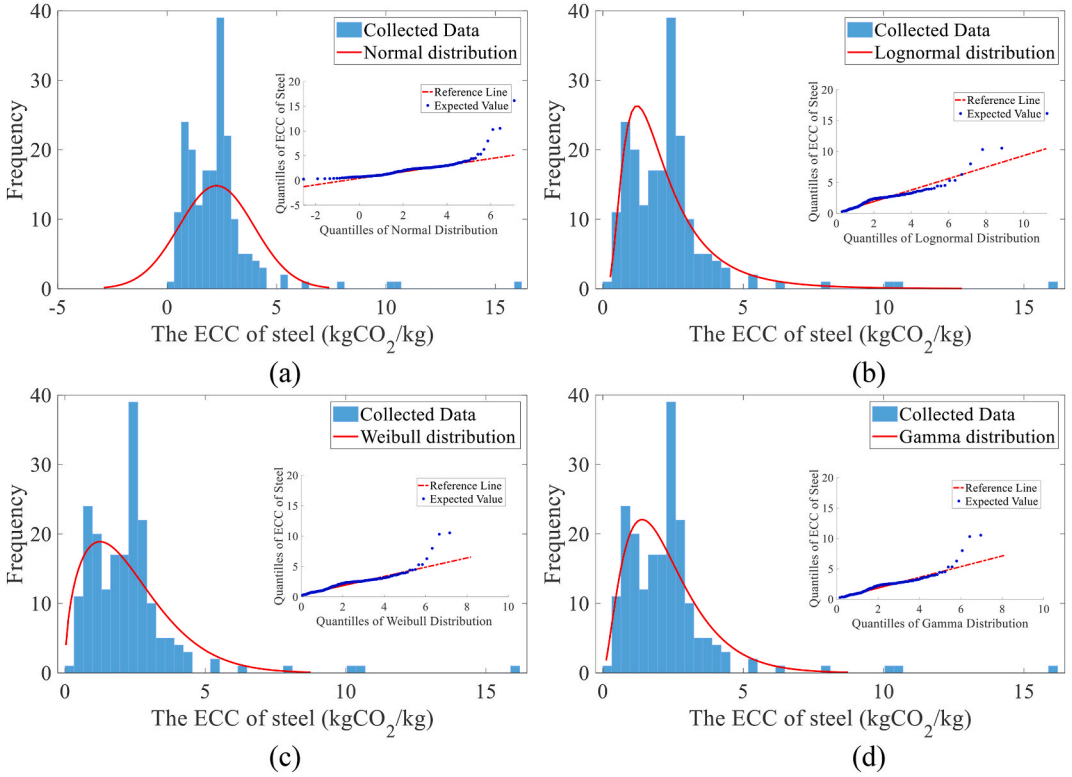

Fig. 3. The distribution fitting for the collected data of ECC of steel against (a) Normal distribution, (b) Lognormal distribution, (c) Weibull distribution, and (d) Gamma distribution.

Table 2
RMSE of the q-q plot for concrete and steel.

Material	Normal	Lognormal	Weibull	Beta	Gamma
Concrete	0.0503	0.0220	0.033	0.0343	-
Steel	1.0326	0.5567	0.7924	-	0.4493

accuracies based on our analysis.

It is worth noting that the proposed RSIDO method in this paper is not dependent on the specific choice of ECC. Moreover, the ECC values are constantly updated due to a variety of factors including material improvements, manufacturing techniques, and policy changes. The proposed method is designed to adapt to such updates, making it applicable under evolving conditions.

2.3. Reliability and sustainability integrated design optimization

In engineering practice, the traditional cost-based and performance-based design objectives are still the primary interest of the design process. To make a structural design with the optimized total embodied carbon, the embodied carbon must be included as a part of the objective function. It can be achieved by applying two normalized weighing factors to form a multi-objective reliability-based design optimization problem. This might provide many possible design outcomes. However, it will further complicate the design process and can create conflicts between the trade-off of two design objectives. Therefore, this paper proposes a reliability and sustainability integrated design optimization (RSIDO) framework. The fundamental idea of the proposed framework is to implement a new probabilistic design constraint to the original problem which bridges the gap between traditional design optimization and sustainability. The new design constraint is related to the total embodied carbon of the interested structure and is selected carefully based on multiple factors. The three staged RSIDO is proposed in this research. The Stage I solves the traditional RBDO problem. Once the optimal design solution is obtained, the probabilistic uncertainty quantification of embodied carbon is conducted as Stage II. Based on the data collection, statistical modelling and Stage I design solution, the probability distribution of the embodied carbon can be estimated. Stage III, the inverse reliability analysis is undertaken to determine the embodied carbon threshold with a set reliability level. Afterwards, the new embodied carbon threshold is developed based on the analysis result. In this work, ϕ is defined as the embodied carbon reduction parameter. The Q_{EC} defines the embodied carbon of the structure. An inverse reliability analysis is con-

ducted to calculate the embodied carbon threshold τ. Thus, the reduced threshold can be computed as $\widehat{Q}_{EC} = \phi \cdot \tau$. By implementing this term as the new design constraint, the problem can be written as follows,

$$\begin{aligned} &\text{Find } \mathbf{d}^{*} \text{ for } \min f(\mathbf{d}) \\ &s.t. \quad \Pr[g_i(\mathbf{X}, \mathbf{d}) \le 0] \le \Phi\left(-\beta_{\text{target},i}\right) \ \text{ for } i = 1, \ldots, n \\ &\Pr[Q_{EC}(\mathbf{X}, \mathbf{d}) \le \widehat{Q}_{EC}] \le \Phi(-\beta_{EC}) \\ &\mathbf{d}_l \le \mathbf{d} \le \mathbf{d}_u \end{aligned} \tag{4}$$

Eq. (4) presents the new problem formulation for the RSIDO Stage III which consists of the probabilistic constraints for both structural performance and embodied carbon requirement. The proposed RSIDO framework facilitates a more holistic approach to structural design by the probabilistic uncertainty quantification of embodied carbon and incorporating it into the optimization process. By using a probabilistic design constraint related to embodied carbon, the framework offers a design method to optimize the design objective without compromising on structural integrity or performance. The RSIDO framework provides several advantages. It integrates structural reliability and embodied carbon reduction seamlessly, addressing both performance and sustainability requirements. By incorporating embodied carbon as a design constraint, the framework ensures that environmental impact is considered in the optimization process, leading to more sustainable outcomes.

The multi-stage process of the RSIDO framework, which includes traditional RBDO, reliability-based embodied carbon quantification, and RSIDO, ensures a comprehensive evaluation at each step. This approach assists in identifying the most efficient design solutions that meet the predefined reliability and sustainability criteria. Additionally, the implementation of the embodied carbon reduction parameter in the design constraint provides a clear metric for sustainability, facilitating easier communication.

Similar to the traditional RBDO for the proposed RSIDO framework, the computational cost is the major challenge as the reliability-based constraints need to be checked for each iteration. This research proposes the use of Active-Learning X-SVR-assisted (AL-X-SVR) RBDO to improve computational efficiency by iteratively selecting new samples and continuously improving the model accuracy of the surrogate model. The detailed algorithms are introduced in the subsequent section.

3. Active learning extended support vector regression

In this section, the framework of the proposed AL-X-SVR for RBDO is introduced and explained in detail. The algorithm of X-SVR is first introduced and followed by the details of the proposed technique.

3.1. Kernelized extended support vector regression

The surrogate modelling technique X-SVR is adopted in this research due to its previous success in structural reliability analysis and uncertainty quantification. The algorithm of X-SVR is presented as follows,

The training datasets $\mathbf{A} = [\mathbf{x}_1, \mathbf{x}_2, \ldots, \mathbf{x}_m]^{\mathrm{T}} \in \Re^{m \times n}$ and $\mathbf{y} = [y_1, y_2, \ldots, y_m]^{\mathrm{T}} \in \Re^{m}$ denote the m sets of training inputs and outputs, respectively, where n denotes the dimension of the input $\mathbf{A}$. The targeted hyperplane $\widehat{g}(\mathbf{x})$, $\mathbf{x} \in \Re^{n}$ can be written as

$$\widehat{g}(\mathbf{x}) = \boldsymbol{\kappa}(\mathbf{x})^{\mathrm{T}}\mathbf{w} + b \tag{5}$$

where $\boldsymbol{\kappa}(\mathbf{x}) \in \Re^{m}$ denotes the kernelized input vector. $\mathbf{w} = [w_1, w_2, \ldots, w_m]^{\mathrm{T}} \in \Re^{m}$ represents the normal to the hyperplane and $b \in \Re$ represents the bias of the hyperplane.

To extend the X-SVR technique to nonlinear problems, the empirical kernel mapping is adopted, which can be expressed as follows,

$$\mathbf{x}_i = [x_{i,1}, x_{i,2}, \ldots, x_{i,n}]^{\mathrm{T}} \rightarrow \boldsymbol{\kappa}(\mathbf{x}_i) = \begin{bmatrix} \boldsymbol{\Phi}(\mathbf{x}_1)^{\mathrm{T}}\boldsymbol{\Phi}(\mathbf{x}_i) \\ \boldsymbol{\Phi}(\mathbf{x}_2)^{\mathrm{T}}\boldsymbol{\Phi}(\mathbf{x}_i) \\ \vdots \\ \boldsymbol{\Phi}(\mathbf{x}_m)^{\mathrm{T}}\boldsymbol{\Phi}(\mathbf{x}_i) \end{bmatrix} = \begin{bmatrix} \kappa(\mathbf{x}_1, \mathbf{x}_i) \\ \kappa(\mathbf{x}_2, \mathbf{x}_i) \\ \vdots \\ \kappa(\mathbf{x}_m, \mathbf{x}_i) \end{bmatrix} \tag{6}$$

where $\boldsymbol{\Phi}(\mathbf{x}_i)$ for $i = 1, 2, \ldots, m$, denotes the kernelized mapping function for transferring the $i-$th training input vector from the original input space $\Re^{n}$ to the high-dimensional empirical space; $\boldsymbol{\kappa}(\mathbf{x}_i)$ denotes the i-th empirical space vector; and $\kappa(\cdot, \cdot)$ denotes Mercer's kernel function.

Thus, for a given kernel function, an arbitrary input vector $\mathbf{x}$ can be transferred into a kernelized input vector $\boldsymbol{\kappa}(\mathbf{x}) \in \Re^{m}$, which is defined as

$$\boldsymbol{\kappa}(\mathbf{x}) = \begin{bmatrix} \kappa(\mathbf{x}_1, \mathbf{x}) & \kappa(\mathbf{x}_2, \mathbf{x}) & \cdots & \kappa(\mathbf{x}_m, \mathbf{x}) \end{bmatrix} \tag{7}$$

Subsequently, the kernelized training input matrix can be calculated as

$$\boldsymbol{\kappa}(\mathbf{A}) = \begin{bmatrix} \kappa(\mathbf{x}_1, \mathbf{x}_1) & \kappa(\mathbf{x}_1, \mathbf{x}_2) & \cdots & \kappa(\mathbf{x}_1, \mathbf{x}_m) \\ \kappa(\mathbf{x}_2, \mathbf{x}_1) & \kappa(\mathbf{x}_2, \mathbf{x}_2) & \cdots & \kappa(\mathbf{x}_2, \mathbf{x}_m) \\ \vdots & \vdots & \ddots & \vdots \\ \kappa(\mathbf{x}_m, \mathbf{x}_1) & \kappa(\mathbf{x}_m, \mathbf{x}_2) & \cdots & \kappa(\mathbf{x}_m, \mathbf{x}_m) \end{bmatrix} \tag{8}$$

Therefore, by further introducing the soft margin ε, the nonlinear X-SVR regression problem with ε-insensitive loss function can be

expressed as,

$$\min_{\mathbf{p},\mathbf{q},b,\boldsymbol{\xi},\boldsymbol{\xi}^*} : \left(\|\mathbf{p}\|_2^2 + \|\mathbf{q}\|_2^2\right) + \gamma \mathbf{e}_n^{\mathrm{T}}(\mathbf{p}+\mathbf{q}) + \frac{C}{2}\left(\boldsymbol{\xi}^{\mathrm{T}}\boldsymbol{\xi} + \boldsymbol{\xi}^{*\mathrm{T}}\boldsymbol{\xi}^*\right)$$
$$s.t. \begin{cases} \boldsymbol{\kappa}(\mathbf{A})(\mathbf{p}-\mathbf{q}) + b\mathbf{e}_m - \mathbf{y} \le \varepsilon \mathbf{e}_m + \boldsymbol{\xi} \\ \boldsymbol{\kappa}(\mathbf{A})(\mathbf{q}-\mathbf{p}) - b\mathbf{e}_m + \mathbf{y} \le \varepsilon \mathbf{e}_m + \boldsymbol{\xi}^* \\ \mathbf{p},\mathbf{q} \ge \mathbf{0}_n;\ \boldsymbol{\xi},\boldsymbol{\xi}^* \ge \mathbf{0}_m \end{cases} \tag{9}$$

where $\mathbf{p}$ and $\mathbf{q}$ consist of non-negative variable vectors; γ is the tuning parameter; C is defined as the penalty constant; the two non-negative vectors $\boldsymbol{\xi} \in \Re^m$ and $\boldsymbol{\xi}^* \in \Re^m$ consist of slack variables; $\mathbf{e}_n = [1,1,\ldots,1]^{\mathrm{T}} \in \Re^n$ and $\mathbf{0}_n = [0,0,\ldots,0]^{\mathrm{T}} \in \Re^n$ denote ones and zeros vectors, respectively.

By manipulating Eq. (9), the constrained optimization problem can be rewritten as

$$\min_{\mathbf{z},b} : \frac{1}{2}\left(\mathbf{z}^{\mathrm{T}}\mathbf{C}\mathbf{z} + b^2\right) + \gamma \mathbf{a}^{\mathrm{T}}\mathbf{z}$$
$$s.t.\ \ (\widehat{\mathbf{A}} + \mathbf{I}_{(2m+2n)\times(2m+2n)})\mathbf{z} + (\varepsilon \mathbf{I}_{(2m+2n)\times(2m+2n)} + b\mathbf{G})\mathbf{b} + \mathbf{d} \ge \mathbf{0}_{4m} \tag{10}$$

where $\mathbf{I}_{(2m+2n)\times(2m+2n)}$ denotes the identity matrix and $\mathbf{C}$, $\mathbf{G}$ and $\widehat{\mathbf{A}} \in \Re^{(2m+2n)\times(2m+2n)}$ are expressed as

$$\mathbf{C} = \begin{bmatrix} \mathbf{I}_{2n\times 2n} & \\ & C\mathbf{I}_{2m\times 2m} \end{bmatrix}, \mathbf{G} = \begin{bmatrix} \mathbf{0}_{2n\times 2n} & \mathbf{0}_{2n\times m} & \mathbf{0}_{2n\times m} \\ \mathbf{0}_{m\times 2n} & \mathbf{I}_{m\times m} & \mathbf{0}_{m\times m} \\ \mathbf{0}_{m\times 2n} & \mathbf{0}_{m\times m} & -\mathbf{I}_{m\times m} \end{bmatrix}, \widehat{\mathbf{A}} = \begin{bmatrix} \mathbf{0}_{2n\times n} & \mathbf{0}_{2n\times n} & \mathbf{0}_{2n\times 2m} \\ -\boldsymbol{\kappa}(\mathbf{A}) & \boldsymbol{\kappa}(\mathbf{A}) & \mathbf{0}_{m\times 2m} \\ \boldsymbol{\kappa}(\mathbf{A}) & -\boldsymbol{\kappa}(\mathbf{A}) & \mathbf{0}_{m\times 2m} \end{bmatrix} \tag{11}$$

$\mathbf{a}, \mathbf{b}, \mathbf{d}$ and $\mathbf{z} \in \Re^{2m+2n}$ can be written as

$$\mathbf{a} = \begin{bmatrix} \mathbf{e}_{2n} \\ \mathbf{0}_{2m} \end{bmatrix}, \mathbf{b} = \begin{bmatrix} \mathbf{0}_{2n} \\ \mathbf{e}_{2m} \end{bmatrix}, \mathbf{d} = \begin{bmatrix} \mathbf{0}_{2n} \\ \mathbf{y} \\ -\mathbf{y} \end{bmatrix}, \mathbf{z} = \begin{bmatrix} \mathbf{p} \\ \mathbf{q} \\ \boldsymbol{\xi} \\ \boldsymbol{\xi}^* \end{bmatrix} \tag{12}$$

By solving the dual problem with the Karush-Kuhn-Tucker (KKT) conditions, the non-negative multiplier $\boldsymbol{\varphi} \in \Re^{2n+2m}$ is introduced. The optimization problem in Eq. (10) can be transformed into a Quadratic Programming (QP) problem, in the form of,

$$\min_{\boldsymbol{\varphi}} : \frac{1}{2}\boldsymbol{\varphi}^{\mathrm{T}}\mathbf{Q}\boldsymbol{\varphi} - \mathbf{m}^{\mathrm{T}}\boldsymbol{\varphi}$$
$$s.t. \quad \boldsymbol{\varphi} \ge \mathbf{0}_{2n+2m} \tag{13}$$

where $\mathbf{Q} \in \Re^{(2m+2n)\times(2m+2n)}$ and $\mathbf{m} \in \Re^{2m+2n}$ are expressed as

$$\mathbf{Q} = (\widehat{\mathbf{A}} + \mathbf{I}_{(2m+2n)\times(2m+2n)})\mathbf{C}^{-1}(\mathbf{A} + \mathbf{I}_{(2m+2n)\times(2m+2n)})^{\mathrm{T}} + \mathbf{G}^{\mathrm{T}}\mathbf{b}\mathbf{b}^{\mathrm{T}}\mathbf{G} \tag{14}$$

$$\mathbf{m} = \gamma(\widehat{\mathbf{A}} + \mathbf{I}_{(2m+2n)\times(2m+2n)})\mathbf{C}^{-1}\mathbf{a} - \varepsilon\mathbf{b} - \mathbf{d} \tag{15}$$

3.2. Active learning extended-support vector regression

The proposed active learning extended-support vector regression (AL-X-SVR) consists of two main stages including global enrichment and local enrichment for the surrogate model construction. Overall, three blocks can be modified including the initial design of experiment (DoE) generation, learning function, and convergence criteria, which are thoroughly presented in **Algorithm 1**.

Algorithm 1. The proposed active-learning extended-support vector regression (AL-X-SVR)

Step 1. Initialization
1.1. Generate a small number of training inputs $[\mathbf{x}_1, \mathbf{x}_2, \ldots, \mathbf{x}_s]^{\mathrm{T}} \in \Re^{s\times n}$ using Latin Hypercube Sampling (LHS);
1.2. Compute the corresponding training outputs following the physical relationship;
1.3. Construct the initial low-fidelity surrogate model $\widehat{g}_0(\mathbf{x})$ through the X-SVR technique and let $i = 0$;
Step 2. Global Enrichment
2.1. Global space-filling training sample generation using LHS;
2.2. Enrichment sample selection based on the learning function $\psi = \left|\widehat{g}_i(\mathbf{x})\right| / d_{\min}$;
2.3. Construct the surrogate model based on $[\mathbf{x}_1, \mathbf{x}_2, \ldots, \mathbf{x}_s, \ldots, \mathbf{x}_i]^{\mathrm{T}} \in \Re^{(s+i)\times n}$.
2.3. If $\left|p_{f,i} - p_{f,i-1}\right| / p_{f,i} < \epsilon_{stage_1}$
2.3.1 Terminate the iteration;
2.4. Else

(*continued on next page*)

(*continued*)

2.4.1 $i = i + 1$ and go back to step 2.2;
2.5. End If.
2.7. Return the last global surrogate model as $\widehat{g}(\mathbf{x}) = \widehat{g}_i(\mathbf{x})$.
Step 3. Local Enrichment
3.1. Solve the RBDO problem with a two-level approach assisted by the global surrogate model and return the design solution $\mathbf{d}_i^*$;
3.2. Local space-filling training sample generation;
3.3. Enrichment sample selection based on the training function in **Step 2.2**;
3.4. Construct the surrogate model;
3.5. Exploitation of unimportant samples $\mathbf{x} \notin [\mu_x - 3\sigma_x, \mu_x + 3\sigma_x] \cup [\mathbf{d}_i^* - 3\sigma_d, \mathbf{d}_i^* + 3\sigma_d]$;
3.6. Solve the RBDO problem with the latest surrogate model and return the design solution $\mathbf{d}_i^*$ and objective value $c_{f,i}$;
3.7. If $|c_{f,i} - c_{f,i-1}| / c_{f,i} < \varepsilon_{stage_2}$
3.1.1 Terminate the iteration;
3.8. Else
3.2.1 $i = i + 1$ and go back to **step 3.3**;
3.9. End If.
3.10. Return the final design solution as $\mathbf{d}_i^*$.

Algorithm 1 illustrates the detailed procedures of the proposed AL-X-SVR-assisted RBDO method. The technique consists of three main steps, i.e., Step 1. Initialization, Step 2. Global enrichment, and Step 3. Local enrichment.

In Step 1 the initialization, a small training sample set is generated. A low-fidelity surrogate model can be constructed based on the limited number of training sets. This initial step consumes only a small number of training samples to catch the overall relationship between structural inputs and response. The LHS is used as the design of the experiment (DoE) method and then the initial surrogate model is constructed using the X-SVR technique.

Afterwards, Step 2, and Step 3 both focus on improving the accuracy of the surrogate model around the vicinity of the limit state function. Step 2 aims to improve the accuracy of the limit state function in the global design space. Firstly, the space-filling training samples are generated in the design space within $[\mu_{\mathbf{x}} - 3\sigma_{\mathbf{x}}, \mu_{\mathbf{x}} + 3\sigma_{\mathbf{x}}]$ for random variables and $[\mathbf{d}_l, \mathbf{d}_u]$ for design variables. These samples are regarded as the candidate pool for selecting the future best samples for surrogate model enrichment. The AL-X-SVR technique seeks to achieve high accuracy of the surrogate model around the vicinity of the limit state function. Fundamentally, selecting the new point is seen as an optimization problem. A learning function is utilized herein to evaluate all the potential low-discrepancy candidate samples and actively select the next training sample. The learning function is defined as,

$$\psi = \frac{|\widehat{g}(\mathbf{x})|}{d_{\min}} \tag{16}$$

where $\widehat{g}(\mathbf{x})$ presents the prediction based on the latest surrogate model. $d_{\min}(\mathbf{x}_s^i)$ denotes the minimum distance between any sample point to all existing training samples in the Euclidean space, which is selected from all distances between the samples in the candidate pool and the existing training sample as $d_{\min}(\mathbf{x}_s^i) = \min\|\mathbf{x}_s - \mathbf{A}_i\|$. This learning function optimizes two objectives which find the sample that is closest to the limit state function and the region has not been explored thoroughly. The proposed method iteratively enriches the accuracy of the surrogate model until the following convergence criterion is met,

$$\frac{\left|p_{f,i} - p_{f,i-1}\right|}{p_{f,i}} < \varepsilon_{stage_1} \tag{17}$$

The convergence criterion is selected as the error of failure events prediction between two iterations. In this work, $\varepsilon_{stage_1} = 5 \times 10^{-4}$ is defined. It is worth noting that the high accuracy of the surrogate model is not compulsory as this step interests in the global structural response approximation. Once the convergence criterion is satisfied, the iteration can be terminated. The method proceeds to the next step.

In Step 2, the AL-X-SVR surrogate model has been enriched globally, which can yield an acceptable design solution. To further improve the accuracy, Step 3 keeps adding new samples into the training datasets with a focus on the important region that is close to the design solution. Firstly, the design solution is found by optimizing the RBDO problem based on the two-level approach assisted by the globally enriched surrogate model. The region of the optimal solution is then selected as the centre of the sampling region for the subsequent local enrichment strategy. The space-filling training samples are generated in the design space following the statistical properties of random variables. For the design variables, the optimal solutions obtained from Step 3.1 are selected as the first statistical moments. The same learning function in Step 2.2 is implemented to select new local enrichment samples. Afterwards, the exploitation of trivial samples is undertaken. As the active-learning strategy focuses on constructing a surrogate model with high accuracy around the limit state function, those previously explored samples far away from the optimal region become insignificant. Further, it demands unnecessary computational costs in the training process and may affect the accuracy of what is truly concerned. Therefore, samples that satisfy $\mathbf{x} \notin [\mu_x - 3\sigma_x, \mu_x + 3\sigma_x] \cup [\mathbf{d}_i^* - 3\sigma_d, \mathbf{d}_i^* + 3\sigma_d]$ is excluded. Then, the surrogate model is constructed based on the new training datasets. The RBDO is solved using the newly updated surrogate model. This process continues until the following convergence criterion is met,

$$\frac{\left|c_{f,i} - c_{f,i-1}\right|}{c_{f,i}} < \varepsilon_{stage_2} \tag{18}$$

The convergence criterion is selected as the error of cost between two subsequent optimized objective function values. In this work, $\varepsilon_{stage_2} = 1 \times 10^{-4}$ is defined. Once the convergence criterion is satisfied, the iteration can be terminated and output the final design solution.

4. Reliability and sustainability integrated design optimization with active learning extended support vector regression

With the assistance of the proposed AL-X-SVR technique, the surrogate model can be effectively constructed to replicate the underlying relationship between the structural inputs and limit state function. The established surrogate model facilitates both RBDO and RSIDO problems. Based on the established surrogate model, the original RBDO and RSIDO problem in Eqs. (1) and (4) can be written as shown in Eqs. (19) and (20).

$$\begin{aligned} &\text{Find } \mathbf{d}^* \text{ for } \min f(\mathbf{X}, \mathbf{d}) \\ &s.t. \quad \Pr[\hat{g}_i(\mathbf{X}, \mathbf{d}) \le 0] \le \Phi(-\beta_{\text{target},i}) \quad \text{for } i = 1, \ldots, n \\ &\mathbf{d}_l \le \mathbf{d} \le \mathbf{d}_u \end{aligned} \tag{19}$$

$$\begin{aligned} &\text{Find } \mathbf{d}^* \text{ for } \min f(\mathbf{d}) \\ &s.t. \quad \Pr[\hat{g}_i(\mathbf{X}, \mathbf{d}) \le 0] \le \Phi(-\beta_{\text{target},i}) \quad \text{for } i = 1, \ldots, n \\ &\Pr[Q_{EC}(\mathbf{X}, \mathbf{d}) \le \hat{Q}_{EC}] \le \Phi(-\beta_{EC}) \\ &\mathbf{d}_l \le \mathbf{d} \le \mathbf{d}_u \end{aligned} \tag{20}$$

where $\hat{g}_i(\mathbf{X}, \mathbf{d})$ denotes the surrogate model for the i-th limit state function with the structural inputs $\mathbf{X}$ and design variables $\mathbf{d}$.

The use of the proposed surrogate modelling technique offers several advantages. First, the adopted X-SVR offers outstanding performance in regression, based on the convex optimization problem. Overfitting is prevented by the embedded hyperparameter auto-tuning and is supported by Bayesian optimization and cross-validation. Furthermore, the use of an active learning strategy with X-SVR increases the sampling efficiency drastically. The surrogate model is compatible with both RDBO and RSIDO. Additionally, surrogate models can continue to be used throughout the entire process of the proposed RSIDO.

In this section, the framework of the RSIDO is presented. The proposed framework has three main stages: Stage I. The AL-X-SVR-

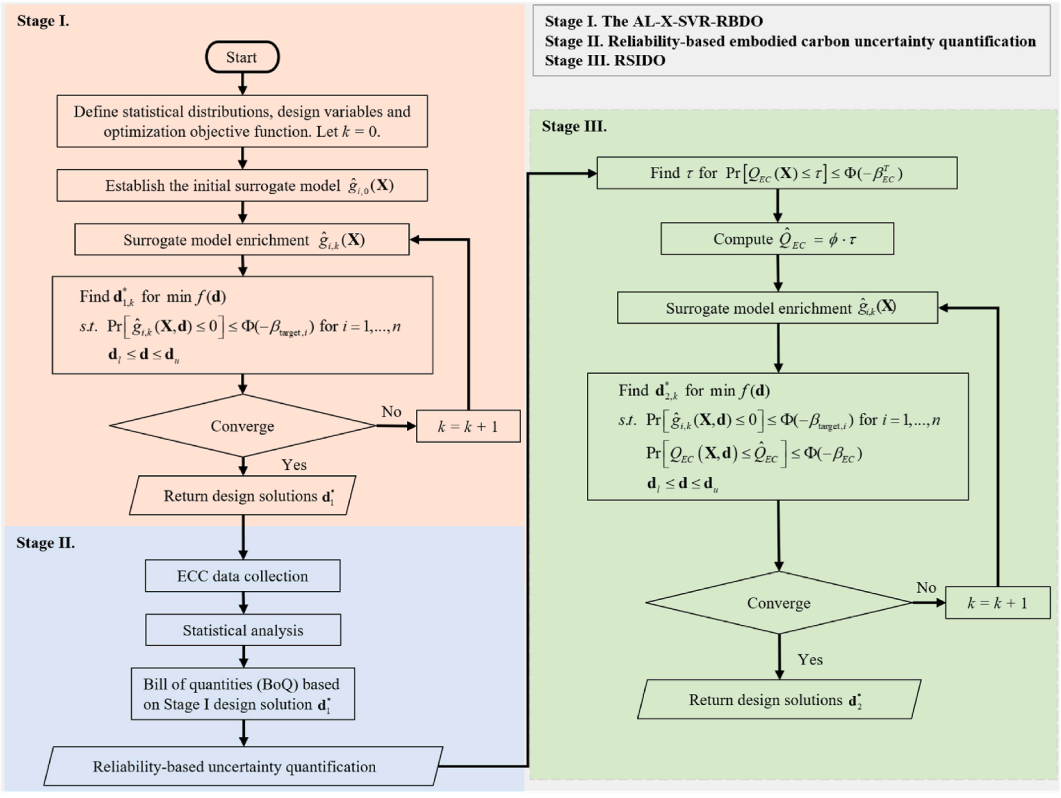

Fig. 4. The flowchart of the RSIDO with active learning machine learning technique.

assisted (AL-X-SVR) RBDO, Stage II. The probabilistic uncertainty quantification of embodied carbon, and Stage III. RSIDO. The detailed framework is illustrated in Fig. 4.

In Stage I. The AL-X-SVR-assisted RBDO, the proposed AL-X-SVR technique is used to solve the classical RBDO problem using a double-loop approach. The first step is to define all statistical properties of random variables, design variables, optimization objectives and probabilistic constraints. Afterwards, the machine learning technique X-SVR is adopted to construct the surrogate model between the structural inputs and response. Different to traditional one-shot sampling strategies, an active-learning scheme is proposed to equip the X-SVR algorithm, namely AL-X-SVR. To improve sampling efficiency, the proposed AL-X-SVR focuses on constructing a surrogate model that is accurate around the limit state function of the RBDO problem. Initially, a small number of training inputs and outputs are generated using the uniform design method by LHS. The first low-fidelity surrogate model can be constructed using the X-SVR technique. To enhance the accuracy of the surrogate model around the limit state function using high-value data points, a low-discrepancy candidate sample pool is generated using the Sobol sequence. Based on the prediction of the previous surrogate model, the next best training point can be computed. The detailed algorithm of AL-X-SVR is introduced in section 3.

Once the RBDO has converged to a design solution, Stage II is the probabilistic uncertainty quantification of embodied carbon based on the design solution provided by Stage I. The three steps to conduct uncertainty quantification of structures include ECC data collection, statistical analysis and sampling of the ECCs for MCS. Afterwards, the probability density function of the interested structure can be estimated. A level of reliability is defined to select the embodied carbon threshold. To further improve the sustainability of the design and decrease the probability of the embodied carbon exceeding the threshold, a threshold reduction factor ϕ can be defined to calculate the new threshold that forms a new RBDO problem as Stage II.

The newly formed RBDO problem is again solved using the proposed AL-X-SVR-assisted RBDO technique. The previously constructed surrogate model in Stage I can still be employed as the probabilistic constraint concerning the implicit limit state function does not change. However, the surrogate model needs further enrichment as the new embodied carbon-related design constraint can cause a shift in the feasible optimal region where the corresponding region of the surrogate model has lower accuracy. Since the surrogate model has converged in the global enrichment stage, it is only required to conduct the local enrichment stage. Unlike the traditional RBDO methods that need to re-run the problem, the high adaptiveness of the proposed method highlights its efficiency. Once the surrogate model converges, the optimal design solution can be computed.

Overall, the proposed RSIDO framework introduces a comprehensive design strategy that simultaneously incorporates sustainable goals, design requirements, and structural reliability. This approach not only combines RBDO with embodied carbon uncertainty quantification but also leverages an innovative active-learning machine learning technique to significantly boost computational efficiency. This advancement represents a shift toward a sustainable design methodology.

5. Numerical validation

To demonstrate the applicability of the proposed AL-X-SVR-assisted RBDO method, a highly nonlinear constraint problem is investigated [32]. This RBDO involves two limit state functions corresponding to two probabilistic constraints. The formulation of this highly nonlinear constraint problem can be written as,

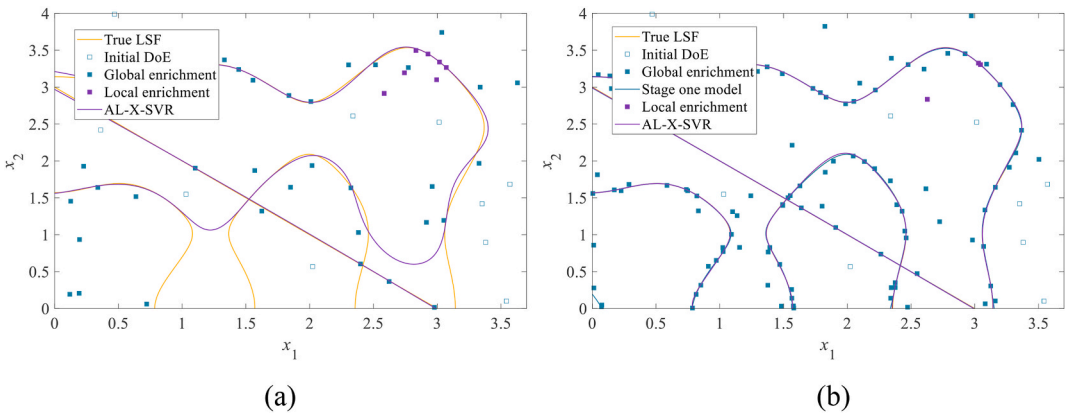

Fig. 5. Result of AL-X-SVR-assisted RBDO with (a) less strict global enrichment convergence criterion, and (b) strict global enrichment convergence criterion.

$$\begin{aligned}
&\min_{\mathbf{d}} : c(\mathbf{d}) = (d_1 - 3.7)^2 + (d_2 - 4)^2 \\
&s.t. : \Pr[g_i(\mathbf{X}(\mathbf{d})) \le 0] \le \Phi\left(-\beta_j^T\right)_i = 1,2 \\
&g_1(\mathbf{X}) = -X_1 \sin(4X_1) - 1.1X_2 \sin(2X_2) \\
&g_2(\mathbf{X}) = X_1 + X_2 - 3 \\
&0 \le d_1 \le 3.7, 0 \le d_2 \le 4 \\
&X_j \sim N\left(d_j, 0.1^2\right), j = 1,2 \\
&\beta_1^T = \beta_2^T = 2
\end{aligned} \tag{21}$$

To demonstrate the effectiveness of the proposed AL-X-SVR-assisted RBDO and the importance of two-stage enrichment, two different convergence criteria are investigated comparably which are $\varepsilon = 0.001$ and $\varepsilon = 0.0001$. The established surrogate models, initial Design of Experiment (DoE), local enrichment and global enrichment points are depicted in Fig. 5.

It can be observed from Fig. 5 (a) and (b), that the relatively higher error threshold for the convergence criterion does not have a significant impact on the convergency of the RBDO problem. On the contrary, the level of error tolerance defined within the convergence criterion is critical as utilizing unnecessary sample points not only consumes unwanted computational cost but also has no increase in the accuracy of the design solution. Therefore, the goal of the global enrichment stage of the proposed method is to construct a low-fidelity surrogate model at first, and as the local enrichment stage initiates, the accuracy of the interested region can be improved iteratively.

For this highly nonlinear constraint problem, the proposed AL-X-SVR-assisted RBDO method generates 10 samples to construct the initial surrogate model. The accuracy of the initial surrogate model is improved iteratively by adding new enrichment samples. Different to traditional SVR and other regression techniques, the selection of the new samples is defined as an optimization problem that seeks to find a new sample that is furthest to all existing samples and closest to the true limit state function. The new learning samples are selected within the generated low-discrepancy sample pool with the help of the learning function. In this case, the Latin Hypercube Sampling (LHS) is utilized to generate the sample pool. Within the framework of the proposed method, two enrichment stages with different convergence criteria and sampling strategies are defined. The first enrichment stage strikes to approximate the global surrogate model with acceptable prediction accuracy around the limit state function. To accelerate the convergence speed, a not-so-strict threshold is selected. This also avoids any unnecessary computational costs being wasted on the suboptimal regions. Subsequently, the double-loop RBDO is performed using the surrogate model. The optimal solution is found and used as the centre of the new sample region for stage two enrichment. In this stage, the LHS is again implemented to generate the sample pool, but new samples follow the statistical properties for all random variables. This enables the finding of the limit state function without exploring suboptimal or unfeasible regions for the RBDO problem. The optimization objective is selected as the convergence criterion for this stage. Once it converges, the result can be returned as the optimal solution.

The result for this highly nonlinear RBDO problem using the proposed method is presented in Table 3. The traditional double-loop RBDO method is adopted as the reference, the Sequential Quadratic Programming (SQP) is selected as the optimization solver for the inner loop and MCS with 1×10^7 iterations are implemented as the outer loop. Other traditional RBDO methods including PMA, and SORA are also compared. Further, surrogate-based method SVR and active-learning Kriging with U-learning function (AK-MCS-U) are undertaken.

As presented in Table 3, both PMA and SORA yield design solutions that do not satisfy the targeted reliability constraint after 2352 and 1539 function evaluations. For surrogate-assisted methods, the design solution given by SVR also fails the reliability constraint after utilizing 200 training data sets. The AK-MCS-U yields a design solution that is much closer to the targeted reliability index for the first constraint after 204 function evaluations for both limit state functions. However, it still fails the reliability requirements of the problem. It is found that the proposed method converges only after consuming 53 function evaluations. The AL-X-SVR only requires 31 and 2 enrichment data points for the first and second limit state functions, respectively. Furthermore, the design solution achieved by the proposed method also indicates the highest agreement with the reference solution. Thus, the applicability and effectiveness of the proposed method is successfully demonstrated.

Table 3
Result of the highly nonlinear RBDO problem.

Method	d_1^*	d_2^*	Cost	β_1^{MCS}	β_2^{MCS}	N
Reference	2.8362-	3.2384	1.3262	2.0000	Inf	$\sim 10^7$
PMA	2.8162	3.2770	1.3038	1.8574	Inf	2352
SORA	2.8162	3.2770	1.3038	1.8574	Inf	1539
SVR	2.9772	3.0814	1.3662	1.7078	Inf	200
AK-MCS-U	2.9580	3.1524	1.2690	1.9349	Inf	204
AL-X-SVR	2.8420	3.2306	1.3281	2.0088	Inf	53

6. Numerical investigations

6.1. Roof truss

To demonstrate the proposed reliability and sustainability integrated design optimization (RSIDO) framework, a roof truss made of concrete and steel is investigated. The roof truss structure is illustrated in Fig. 6.

For the roof truss shown in Fig. 6, the upper part of the structure in compression is made of concrete and the lower part in tension is made of steel. The cross-sectional area of concrete members and steel members are A_c and A_s, respectively. The Young's modulus for concrete and steel are denoted as E_c and E_s, respectively. P denotes the equivalent concentrated nodal load which can be calculated by $ql/4$. The q denotes the uniformly distributed load on the roof truss and the l denotes the total span of the roof truss. The serviceability limit state is defined where the maximum allowable displacement is set to be 0.03 m. The proposed RSIDO framework implements a traditional RBDO as the first stage where the RBDO formulation can be written as,

$$\begin{aligned} &\min_{\mathbf{d}} \ m(\mu_{A_c}, \mu_{A_s}) \\ &s.t. \ \ \Pr[g(\mathbf{d}, \mathbf{X}) \le 0] \le \Phi(-\beta^T) \\ &g = 0.03 - \left(\frac{ql^2}{2}\right)\left(\frac{3.81}{A_c E_c} + \frac{1.13}{A_s E_s}\right) \\ &0.018 \le \mu_{A_c} \le 0.063, 6 \times 10^{-4} \le \mu_{A_s} \le 1.2 \times 10^{-3}, \beta^T = 3 \end{aligned} \tag{22}$$

The RBDO formulation shown in Eq. (1) involves optimizing the total mass of the structure while satisfying the probabilistic constraint. The design variables are the cross-sectional area of concrete and steel members, respectively. The targeted reliability index is defined as 3. The statistical properties of all variables are provided in Table 4.

For the investigated roof truss, the result of the proposed AL-X-SVR-assisted RBDO is presented in Table 5. The double-loop crude MCS with 1×10^7 iterations is selected as the reference. Additionally, results of other traditional RBDO algorithms, SVR, and AK-MCS-U techniques are also tabulated for comparison.

As presented in Table 5, both PMA and SORA yield design solutions that do not satisfy the targeted reliability constraint. Furthermore, the PMA and SORA utilize a much larger number of function evaluations. For surrogate-assisted methods, the SVR trained using 200 data sets also yields a design solution that does not satisfy the reliability constraint. The AK-MCS-U provides an acceptable design solution where the reliability constraint is met and costs 68 function evaluations. However, it is observed that the design solution by AK-MCS-U is too conservative as it exceeds the actual targeted reliability index and makes the structure heavier than the reference. Therefore, the optimal result is not obtained. It is found that the proposed method obtains an accurate design solution by only consuming 91 function evaluations for this problem and yields a design solution with a reliability index of 3.0435. Furthermore, the best design objective is achieved by the proposed method. The design solution solved using the AL-X-SVR is also the closest to the reference value amongst the surrogate-based RBDO methods, which further highlights the effectiveness and efficiency of the proposed method.

To incorporate embodied carbon quantification, the probabilistic uncertainty quantification of embodied carbon of the roof truss is investigated based on the previously optimized solution. A new embodied carbon reduction threshold is determined based on the probability distribution of the total embodied carbon of the structure. As a result, a new probabilistic constraint is added to the original RBDO problem. The total mass of the structure is still adopted as the design objective of the roof truss structure in the following section, and the formulation of Stage III can be written as,

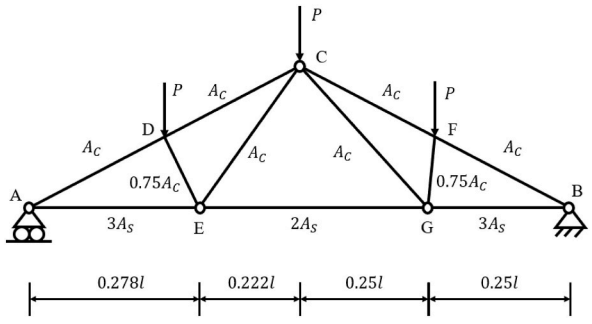

Fig. 6. The numerical model of the roof truss structure [33].

Table 4
Statistical properties of design and random variables.

Statistical Information	q(N/m)	l(m)	A_s(m^2)	A_c(m^2)	E_s(GPa)	E_C(GPa)
Mean	20000	12	Design variable	Design variable	100	20
Standard deviation	1400	0.12	5.9852×10^{-5}	4.8×10^{-3}	6	1.2

Table 5
The result of the RBDO of the roof truss.

Method	d_1^* ($\times 10^{-3}$ m^2)	d_2^* ($\times 10^{-2}$ m^2)	Mass (kg)	β_{MCS}	N
Reference	1.2000	3.4768	2045.452	3	$\sim 10^7$
PMA	1.2000	3.4215	2017.495	2.9164	2786
SORA	1.2000	3.4215	2017.495	2.9164	721
SVR	1.2000	3.3730	1992.909	2.8417	200
AK-MCS-U	1.2000	3.7384	2177.545	3.3776	68
AL-X-SVR	1.2000	3.5073	2060.925	3.0435	91

$$\begin{aligned} &\min_{\mathbf{d}} \; m\left(\mu_{A_c}, \mu_{A_s}\right) \\ &s.t. \;\; \Pr[g(\mathbf{X}, \mathbf{d}) \le 0] \le \Phi\left(-\beta^T\right) \\ &\Pr[Q_{EC}(\mathbf{X}, \mathbf{d}) \le \widehat{Q}_{EC}] \le \Phi\left(-\beta_{EC}^T\right) \\ &g = 0.03 - \left(\frac{ql^2}{2}\right)\left(\frac{3.81}{A_c E_c} + \frac{1.13}{A_s E_s}\right) \\ &0.018 \le \mu_{A_c} \le 0.063, 6 \times 10^{-4} \le \mu_{A_s} \le 1.2 \times 10^{-3}, \beta^T = 3 \end{aligned} \tag{23}$$

In Eq. (23), the design objective remains unchanged, where the $Q_{EC}(\mathbf{X}, \mathbf{d})$ and $\widehat{Q}_{EC}$ denote the total embodied carbon of the structure and the new targeted embodied carbon threshold. The targeted reliability index for the embodied carbon constraint is also selected as 3. The design solutions are tabulated in Table 6.

It can be seen from Table 6, that design outcomes for Stage III of the proposed RSIDO by various methods are presented. The traditional RBDO methods PMA and SORA provide identical design solutions. The PMA method consumes 66416 function evaluations and SORA consumes 2627 function evaluations. The surrogate model-assisted methods utilize significantly less number of function evaluations. The SVR method trained using 200 data sets gives a design solution with acceptable accuracy. The AK-MCS-U method converges with 272 training samples and yields a solution. However, it does not satisfy the two reliability constraints very well. Using the proposed AL-X-SVR technique, 10 initial training samples are generated and the surrogate model converges with only 84 enrichment iterations. Furthermore, the accuracy is demonstrated against the reference value.

From this case study, the proposed RSIDO framework is demonstrated which implements a traditional RBDO as the first stage. Afterwards, a new probabilistic design constraint is introduced based on the embodied carbon quantification result of the previously solved optimization problem. The optimal solution is obtained using the proposed AL-X-SVR technique whose accuracy was tested against other RBDO methods. Then, the probabilistic uncertainty quantification of embodied carbon of the designed structures is carried out. Based on the probability distribution of the total embodied carbon, the concept of reliability is utilized to select a reduced threshold for the embodied carbon as a design requirement. In this case, a 5 % reduction is selected for the interested structure.

Lastly, the uncertainty quantification of the embodied carbon for Stage I and Stage III is depicted to show the embodied carbon distribution from the two designs.

In Fig. 7, the uncertainty quantification of the three stages of the proposed RSIDO method is demonstrated. The histogram of total embodied carbon across the three stages: Initial design values, Stage I RBDO result, and Stage III RSIDO result which provides a clear visualization of how the design evolves to improve the embodied carbon distribution while maintaining structural performance. It can be observed that the initial design variable poses the greatest amount of embodied carbon. Furthermore, the embodied carbon distribution of the initial stage decays more slowly in the upper tail, implying a higher probability of large embodied carbon values

Table 6
The result of the RSIDO for the roof truss.

Method	d_1^* ($\times 10^{-3}$ m^2)	d_2^* ($\times 10^{-2}$ m^2)	Mass (kg)	Embodied Carbon (kg)	β_{MCS}	β_{EC}	N
Reference	1.0610	4.0959	2325.758	912.5735	2.9992	3.0002	$\sim 10^7$
PMA	1.2000	3.4215	2017.495	930.9627	2.9164	2.8548	66416
SORA	1.2000	3.4215	2017.495	930.9627	2.9164	2.8548	2627
SVR	1.0740	4.0087	2284.789	912.4405	3.0034	2.9863	200
AK-MCS-U	1.2000	3.4401	2026.884	932.4974	2.9443	2.9017	272
AL-X-SVR	1.1045	4.2126	2381.017	913.7644	2.99215	3.0007	94

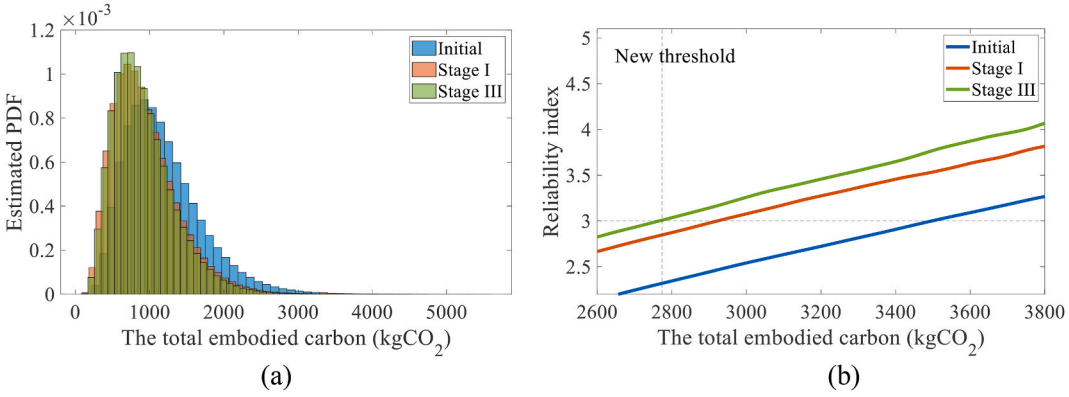

Fig. 7. (a) The histogram of the total embodied carbon, and (b) the reliability index against the embodied carbon level of the roof truss for Initial Stage, Stage I, and Stage III.

compared to the other distribution. This spread reflects that the preliminary design's lack of optimization, leading to inefficient material use and higher carbon emissions. The large variance suggests that the design is overly conservative, accounting for uncertainties but at the expense of higher embodied carbon levels. After applying Stage I RBDO, the distribution of total embodied carbon becomes more concentrated towards lower values. This indicates that the RBDO process effectively reduces the embodied carbon by optimizing the design variables, while still satisfying reliability constraints. The shift in the distribution illustrates an improvement over the initial design. Lastly, Stage III further sharpens the embodied carbon distribution. The histogram shows a narrower spread of total embodied carbon values, with the distribution shifting further towards the end. This reflects the advantages provided by the proposed RSIDO method as the new design solution reduces variance compared to the last stage.

In Fig. 7 (b), the embodied carbon threshold versus reliability index across the three stages are plotted. For the initial design, the reliability index curve is low, indicating the design with a higher likelihood of exceeding the embodied carbon threshold. After Stage I, it is found that the curve is shifted upwards with an increase in the reliability index. However, the probabilistic constraint regarding the embodied carbon threshold has not been met even after Stage I. It is observed that the Stage III design perfectly satisfies the probabilistic constraint of the embodied carbon. The connection between material usage and embodied carbon becomes especially evident when the three stages are compared. While structural performance is fulfilled by all three designs, changes in the quantity of material used have a notable effect on the distribution of embodied carbon. As the design evolves from the initial stage to the Stage I RBDO and Stage III RSIDO, the material is utilized more efficiently, leading to a reduction in embodied carbon without compromising structural reliability. This highlights the importance of material selection and its impact on sustainability in the design process. Throughout the design process, the sustainability aspect is considered within the reliability constraint. The RSIDO is solved using a two-stage strategy where the first stage executes the original RBDO problem to select the sustainability threshold and the second stage solves the newly formed problem. In this approach, the original objective is still solely the interested value for optimization, but the concept of reliability is implemented in a sustainable way to limit the probability of embodied carbon exceeding the defined threshold.

6.2. *Reinforced concrete beam*

To investigate the practicality of the proposed method for engineering problems, a reinforced concrete beam is studied. The model of the reinforced concrete beam is depicted in Fig. 8.

For the reinforced concrete beam depicted in Fig. 8, the beam is simply supported on two ends. The finite element method (FEM) is adopted for the analysis of the reinforced concrete beam. The steel reinforcement bars are modelled using truss elements to avoid

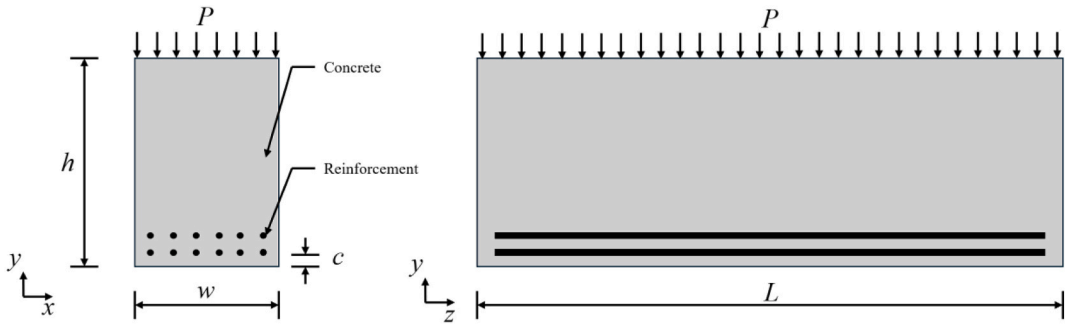

Fig. 8. The reinforced concrete beam.

redundant computational costs. To achieve model accuracy, a convergence study has been undertaken which indicates discretising the structure into 4896 elements with 38896 degrees of freedom (DoF) is sufficient. The beam itself is L in length, w in width, and h in height. The top surface is under static loading with the magnitude of P. Two layers of six steel reinforcement bars are embedded in the bottom part of the concrete with a cover depth c of 25 mm. The diameter of the rebar is denoted as d, and the Young's modulus of concrete and steel are denoted as E_c and E_s, respectively. The cross-sectional area is selected as the optimization objective. The maximum allowable displacement of the reinforced concrete beam is selected as the limit state function in this example, which the RBDO problem can be expressed as,

$$\begin{aligned}
&\min_{\mathbf{d}} \ A(\mu_w, \mu_h, \mu_d) \\
&s.t. \ \ \Pr[g(\mathbf{d}, \mathbf{X}) = g(\mu_w, \mu_h, \mu_d, P, E_c, E_s) \le 0] \le \Phi(-\beta^T) \\
&g(\mathbf{d}, \mathbf{X}) = g(\mu_w, \mu_h, \mu_d, P, E_c, E_s) = 0.008 - \Delta(\mu_w, \mu_h, \mu_d, P, E_c, E_s) \\
&600 \ \text{mm} \le \mu_w \le 1000 \ \text{mm}, 800 \ \text{mm} \le \mu_h \le 1200 \ \text{mm}, 8 \ \text{mm} \le \mu_d \le 30 \ \text{mm} \\
&\beta^T = 3
\end{aligned} \tag{24}$$

The RBDO formulation shown in Eq. (24) involves optimizing the cross-sectional area of the beam while satisfying the reliability constraint. The design variables are the width, height of the beam and diameter of the steel reinforcement bars. The targeted reliability index is defined as 3. The statistical properties of all variables are provided in Table 7.

For the investigated reinforced concrete beam, the result for Stage I of the proposed RSIDO is presented in Table 8. Other traditional RBDO methods including PMA, and SORA are also compared. Additionally, surrogate-based methods including SVR and AK-MCS-U are also conducted.

From Table 8, the double loop MCS fails to converge due to the operationally infeasible computational costs. The PMA provides a solution with a reliability index of 2.0697 by computing the original function 1960 times. The SORA provides a solution with a reliability index of 2.9955 and 428 original functions are evaluated. To investigate the surrogate model-based approaches, SVR, AK-MCS-U, and AL-X-SVR are compared. The SVR takes 1000 randomly generated training data sets within the design space which yields a design solution that fails the reliability constraint. 10 initial training samples are generated for both AK-MCS-U and AL-X-SVR. It is found that the AK-MCS-U utilizes an additional 46 sample points to converge, whereas the proposed method takes 43 enrichment points. It can be seen that the two methods consume very close computational costs, and the efficiency is significantly increased compared to traditional RBDO methods. Further, the result indicates that the proposed AL-X-SVR provides a design solution with a reliability index of 2.9314 and the AK-MCS-U provides a design solution with a reliability index of 3.3636. From the three design solutions given by SORA, AK-MCS-U and AL-X-SVR, the AL-X-SVR gives the best outcome with optimal design objective. This again highlights the effectiveness of the proposed AL-X-SVR technique.

To incorporate the embodied carbon, the probabilistic uncertainty quantification of embodied carbon of the reinforced concrete beam is investigated based on the previously optimized solution. A new embodied carbon reduction threshold is determined based on the probability distribution of the total embodied carbon of the structure. As a result, a new probabilistic constraint is added to the original RBDO problem.

From the Stage I results, the uncertainty quantification of embodied carbon can be carried out. The reduction parameter is selected based on the quantification result, which is 3 % for this case. Once the new embodied carbon reduction threshold is determined, it is implemented as the probabilistic constraint to the original RBDO problem. The cross-sectional area is still adopted as the design objective of the reinforced concrete beam in the following section, and the formulation of Stage III can be found in Eq. (A1) in the Appendix.

For the investigated reinforced concrete beam, the result of the proposed RSIDO is presented in Table 9. Other traditional RBDO methods including PMA, and SORA are also compared. Additionally, surrogate-based methods including SVR and AK-MCS-U are also compared.

It can be seen from Table 9, that design outcomes for Stage III of the proposed RSIDO by various methods are presented. The traditional RBDO methods PMA and SORA provide identical design solutions. The PMA method consumes 7342 function evaluations and SORA consumes 1157 function evaluations. It is observed that the surrogate model-assisted methods utilized far less number of function evaluations. The SVR model is trained using 1000 randomly generated samples, and the yielded design solution fails to satisfy the reliability constraint. The AK-MCS-U method converges with 60 training samples and yields a solution. However, it does not satisfy the reliability constraint as well. Using the proposed AL-X-SVR technique, the surrogate model converges with only 55 iterations. Furthermore, the reliability index of the final design solution is close to the reliability requirement.

Table 7
Statistical properties of design and random variables.

Variable	Description	Distribution	Mean	Standard deviation
P (kN)	Load	Gumbel	1920	192
w (mm)	Width	Normal	Design variable	17.5
h (mm)	Height	Normal	Design variable	10
L (mm)	Length	Deterministic	8000	–
d (mm)	Diameter	Normal	Design variable	0.4
E_c (GPa)	Young's modulus	Normal	25	1.25
E_s (GPa)	Young's modulus	Normal	200	10

Table 8
The result of the RBDO for the reinforced concrete beam.

Method	d_1^* ($\times 10^{-1}$ m)	d_2^* ($\times 10^{-1}$ m)	d_3^* (mm)	Area ($\times 10^{-1}$ m^2)	β_{IS}	N
PMA	6.0007e	8.7929	29.9793	5.2763	2.0697	1960
SORA	6.0164	8.8176	29.4831	5.3050	2.9955	1157
SVR	6.0000	8.0000	26.0786	4.8000	1.0606	1000
AK-MCS-U	6.0162	9.2991	20.0159	5.5945	3.3636	56
AL-X-SVR	6.0000	8.7656	30.0000	5.2593	2.9314	53

Table 9
The result of the RSIDO for the reinforced concrete beam.

Method	d_1^* ($\times 10^{-1}$ m)	d_2^* ($\times 10^{-1}$ m)	d_3^* (mm)	Area ($\times 10^{-1}$ m^2)	Embodied Carbon (kg)	β_{IS}	N
PMA	6.0033	8.7969	29.8974	5.2811	1420.107	2.9725	7342
SORA	6.0033	8.7969	29.8974	5.2811	1402.109	2.9725	1157
SVR	6.0000	8.0002	25.4046	4.8012	1181.788	1.0143	1000
AK-MCS-U	6.0000	8.0000	19.0010	4.8000	995.7882	0.5497	60
AL-X-SVR	6.0000	8.8754	26.2327	5.3252	1292.684	2.9311	55

6.3. RC slab

A reinforced concrete slab is studied to investigate the effectiveness of the proposed method for engineering problems further. The model of the reinforced concrete slab is depicted in Fig. 9.

For the reinforced concrete slab depicted in Fig. 9, the slab is fixed on all edges. The slab is analysed using the FEM. To achieve model accuracy, a convergence study has been undertaken which indicates discretising the structure into 15160 elements with 136060 degrees of freedom (DoF) is sufficient. The two sides are L in length and h in height. The top surface is under static loading with the magnitude of P. Two layers of reinforcement bars are embedded in the bottom part of the concrete with a cover depth c of 25 mm, which is perpendicular to each other. The diameter of the rebar is denoted as d, and the Young's modulus of concrete and steel are denoted as E_c and E_s, respectively. Additionally, the f_c and f_s denote the concrete compressive strength and steel initial yield stress, respectively. The isotropic tangent modulus is defined as E_t. The mass of the investigated reinforced concrete slab is selected as the optimization objective. The maximum allowable displacement of the structure is selected as the limit state function in this example, which the RBDO problem can be expressed as,

$$\begin{aligned} &\min_{\mathbf{d}} \ m(\mu_d, \mu_h) \\ &s.t. \ \ \Pr[g(\mathbf{d}, \mathbf{X}) = g(\mu_d, \mu_h, P, E_c, E_s, f_c, f_s, E_t) \le 0] \le \Phi(-\beta^T) \\ &g(\mathbf{d}, \mathbf{X}) = 0.01 - \Delta(\mathbf{d}, \mathbf{X}) \\ &8\text{mm} \le \mu_d \le 20\text{mm}, 50\text{mm} \le \mu_h \le 300\text{mm} \\ &\beta^T = 3 \end{aligned} \tag{25}$$

The RBDO formulation shown in Eq. (26) involves optimizing the mass of the slab while satisfying the reliability constraint. The design variables are the height of the slab and the diameter of the steel reinforcement bars. The targeted reliability index is defined as

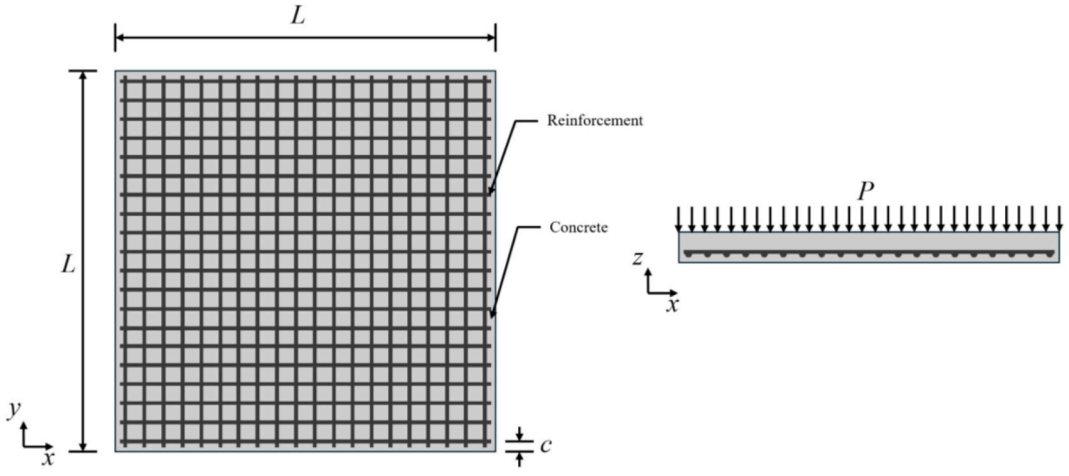

Fig. 9. The model of the reinforced concrete slab.

3. The statistical properties of all variables are provided in Table 10.

For the investigated reinforced concrete slab, the proposed RSIDO is presented in Table 11. Other traditional RBDO methods including PMA, and SORA are also compared. Additionally, surrogate-based methods including SVR and AK-MCS-U are also conducted.

The double loop MCS fails to converge due to the operationally infeasible computational costs. For Stage I, the PMA provides a solution with 1602 times of original functions. The SORA provides a solution with 428 original functions evaluated. To investigate the surrogate model-based approaches, SVR, AK-MCS-U, and AL-X-SVR are compared. The SVR takes 200 randomly generated training data sets within the design space which yields a design solution. 10 initial training samples are generated for both AK-MCS-U and AL-X-SVR. It is found that the AK-MCS-U utilizes 42 sample points to converge, whereas the proposed method takes 112 enrichment points. It can be seen that the two methods significantly increase the computational efficiency compared to traditional RBDO methods. To incorporate the embodied carbon, the probabilistic uncertainty quantification of the embodied carbon of the reinforced concrete slab is investigated based on the previously optimized solution. Following the proposed framework, from the Stage I results, the uncertainty quantification of embodied carbon can be carried out. The reduction parameter is selected based on the quantification result, which is 3 % for this case. Once the new embodied carbon reduction threshold is determined, it is implemented as the probabilistic constraint to the original RBDO problem. The mass is still adopted as the design objective of the reinforced concrete slab in the following section, and the formulation of Stage III can be found in Eq. (A2) in the Appendix.

It is observed from Table 11, that design outcomes for Stage III of the proposed RSIDO by various methods are presented. The traditional RBDO methods PMA and SORA provide identical design solutions. The PMA method consumes 10087 function evaluations and SORA consumes 593 function evaluations. It is observed that the surrogate model-assisted methods utilized far less number of function evaluations. The SVR model is trained using 200 randomly generated samples, and the yielded design solution fails to satisfy the reliability constraint. The AK-MCS-U method converges with 152 training samples and yields a solution. Using the proposed AL-X-SVR technique, the surrogate model converges with only 20 iterations. The design solutions given by AK-MCS-U and AL-X-SVR highly agree with each other. However, the performance of AL-X-SVR is slightly superior to AK-MCS-U due to the lower computational cost.

7. Discussion

The proposed reliability and sustainability integrated design optimization (RSIDO) framework presents a design approach that addresses sustainability, design objectives and structural performance simultaneously. This work not only integrates reliability-based design optimization (RBDO) with embodied carbon quantification but also implements a novel active learning machine learning technique to enhance computational efficiency, signifying a development towards a sustainable methodology in design optimization with the consideration of structural reliability.

The RSIDO framework incorporates embodied carbon as a design constraint which allows the environmental impact to be mitigated. The three stages approach facilitates a stepwise integration with structural performance and embodied carbon, beginning with the established RBDO framework, followed by the embodied carbon threshold selection based on the embodied carbon uncertainty quantification. Lastly, a new probabilistic design constraint related to embodied carbon is implemented in the original RBDO to form a new optimization problem. To achieve accurate results for probabilistic uncertainty quantification of embodied carbon, it is important to develop appropriate statistical models. In this study, the cradle-to-gate stages, including raw material extraction, transportation, and manufacturing, were taken into account for the most two common construction materials, concrete and steel. Using the data gathered, statistical models for the embodied carbon coefficients (ECCs) were developed through maximum likelihood estimation (MLE) distribution fitting, utilizing 120 and 197 data points for concrete and steel, respectively. These statistical models facilitate precise decision-making and provide a foundation for the proposed framework. It is noteworthy that these are constantly evolving due to changes in various factors. However, the RSIDO can adapt to different ECCs.

7.1. Embodied carbon results

The effectiveness of the proposed RSIDO has been demonstrated using the numerical investigations including roof truss, reinforced concrete beam and reinforced concrete slab. In this section, the results of the embodied carbon using RSIDO by different RBDO algorithms are compared.

In the roof truss analysis, the proposed AL-X-SVR technique achieved an embodied carbon value of 913.7644 kg, which is slightly higher than the reference value of 912.5735 kg but significantly lower than the Performance Measure Approach (PMA) and Sequential Optimization and Reliability Assessment (SORA) with the embodied carbon of 930.9627 kg. This result demonstrates that the RSIDO framework, supported by the AL-X-SVR technique, achieves an embodied carbon reduction comparable to the reference design, which represents an optimal design solution. This efficiency in embodied carbon reduction are beneficial when scaling to larger structures or multiple roof truss components, as the RSIDO approach reduces material waste and embodied carbon without compromising the structure's intended functionality or safety.

For the reinforced concrete beam, the embodied carbon value by the AL-X-SVR was yielded as 1292.684 kg which is lower than the PMA and SORA with embodied carbon of 1402.109 kg, highlighting a significant advantage compared to the traditional FORM-based methods. In the reinforced concrete slab, both the active-learning Kriging with U-learning function (AK-MCS-U) and AL-X-SVR methods yielded comparable results 2302.1 kg and 2296.3 kg, respectively. However, the PMA and SORA both yield 2709.8 kg which lead to significant embodied carbon compared to design solutions given by AL-X-SVR and AK-MCS-U.

Overall, the RSIDO framework's applicability to these structure types has been well demonstrated which showcases its capabilities

Table 10
Statistical properties of design and random variables.

Variable	Description	Distribution	Mean	Standard deviation
P (kN)	Load	Gumbel	70	7
d (mm)	Diameter	Normal	Design variable	0.4
h (mm)	Height	Normal	Design variable	8
L (mm)	Length	Deterministic	8000	–
E_c (GPa)	Young's modulus	Normal	25	1.25
E_s (GPa)	Young's modulus	Normal	200	10
f_c (MPa)	Concrete compressive strength	Normal	20	2
f_s (MPa)	Steel initial yield stress	Normal	100	10
E_t (GPa)	Isotropic tangent modulus	Normal	20	2

Table 11
The result of the RSIDO for the reinforced concrete slab.

Method	d_1^* ($\times 10^{-3}$ m)	d_2^* ($\times 10^{-1}$ m)	Mass ($\times 10^3$ kg)	Embodied Carbon ($\times 10^3$ kg)	N
PMA	20.0000	1.0000	9.0441	2.7098	1602 + 10087
SORA	20.0000	1.0000	9.0441	2.7098	428 + 593
SVR	8.0000	1.0000	8.7047	1.6304	200 + 200
AK-MCS-U	8.0062	1.4672	12.7416	2.2963	152 + 42
AL-X-SVR	8.0003	1.4714	12.7774	2.3021	122 + 20

to regulate embodied carbon emissions while considering structural reliability. By targeting embodied carbon as a key probabilistic optimization constraint, RSIDO promotes more sustainable design choices that reduce the overall embodied carbon of construction projects.

7.2. Performance of AL-X-SVR

In RBDO, the computational burden associated with reliability analysis is seen as one of the biggest challenges, especially when time-consuming structural model is encountered. For traditional RBDO, the Monte Carlo Simulation (MCS) is employed to run the reliability analysis for each iteration of optimization. This computational burden of performing MCS based on the original physical model can be very costly for a single reliability analysis. Conducting for all iterations of optimization will significantly increase the computational time and eventually become infeasible for complex physical models. To mitigate this challenge, we utilize a surrogate model to replace the original time-consuming structural model. In this way, the RBDO remains computationally feasible for complex structures. The active-learning extended-support vector regression (AL-X-SVR) technique is proposed in this paper which addresses this challenge by iteratively refining the surrogate model, enhancing accuracy with fewer training samples. The two-level enrichment strategy enables the model to focus on regions of interest and reduces computational costs.

The applicability and effectiveness of the AL-X-SVR have been demonstrated using a highly nonlinear constrained RBDO problem, roof truss, reinforced concrete beam and reinforced concrete slab. It was observed that the AL-X-SVR outperforms traditional methods such as MCS, PMA, SORA, and other machine learning techniques including Support Vector Regression (SVR), and AK-MCS-U. Traditional methods struggle to overcome computational limitations as the limited state function becomes time-consuming. For the PMA and SORA, the results are often inaccurate compared to the machine learning-assisted methods due to the nature of methods as they utilize First Taylor Expansion to approximate the limit state function. For this reason, the design result often fails to meet the actual probabilistic constraints for structures with highly nonlinear limit state functions. Furthermore, the AL-X-SVR technique demonstrates better performance and accuracy than the SVR and AK-MCS-U while using fewer training samples.

The successful application of the proposed RSIDO framework inspires future research works, potentially extending beyond building components to full-size buildings with more design variables.

8. Conclusion

In this study, the reliability and sustainability integrated design optimization (RSIDO) framework for engineering structures was proposed. The embodied carbon coefficients (ECCs) were collected for two common construction materials: concrete and steel. Based on the data collection, the statistical models of ECCs were established via maximum likelihood estimation (MLE) distribution fitting based on the collected 120 and 197 data points for concrete and steel, respectively. These credible statistical models enable accurate decision-making and lay the foundation for the proposed RSIDO. The RSIDO framework consists of three main stages. Stage I is the classical RBDO problem. Stage II is the reliability-based embodied carbon quantification. Stage III calculates the embodied carbon reduction threshold based on the quantification result. The reduction threshold value was adopted as a reliability-based design constraint to form the new RSIDO problem. The optimization process is computationally expensive, especially for complex, implicit physical problems. The Extended Support Vector Regression (X-SVR) was adopted as the surrogate modelling technique to represent the relationship between structural inputs and interested responses. Furthermore, this study proposed an active learning strategy to

improve the efficiency of X-SVR, namely the Active-Learning X-SVR-assisted RBDO (AL-X-SVR-RBDO). The active learning module ensures the training samples are added to the critical region for each iteration. The proposed AL-X-SVR-RBDO was adopted throughout the RSIDO which can drastically improve the optimization efficiency. The applicability of the proposed AL-X-SVR was validated using a highly nonlinear constraint mathematical RBDO problem. It was observed that the proposed AL-X-SVR-RBDO method significantly reduces the computational costs compared to the classical RBDO methods. Additionally, the two-stage global and local enrichment strategy embedded in the AL-X-SVR-RBDO avoided sampling excessively in the sub-optimal region within the design space.

Three engineering applications were investigated to demonstrate the effectiveness and efficiency of the proposed RSIDO framework. From the three engineering applications, the proposed AL-X-SVR-RBDO was used as the surrogate modelling technique and its efficiency was also demonstrated. From the three investigations, it can be found that the three stages of the proposed RSIDO all contribute to embodied carbon reduction. Stage I solved the RBDO which often has design objectives such as cost and mass. This step was the foundation of the RSIDO as it provides a design solution while satisfying the structural performance. In practice, the design objective might be strongly correlated with the total embodied carbon of the structure. Therefore, carbon reduction can be observed within the first step for all investigated structures after Stage I. Stage II, the reliability-based embodied carbon quantification utilized the established statistical models of ECCs and the design solution. An inverse reliability analysis problem was defined to determine the new embodied carbon threshold for the concerned structure. Stage III implemented the new embodied carbon threshold as a probabilistic constraint to form the RSIDO problem. The AL-X-SVR was adopted in both Stage I and Stage III. It was found that generally the proposed AL-X-SVR yields accurate predictions of the limit state and consumes fewer training samples compared to other surrogate models.

Overall, the proposed RSIDO provides a new design approach by integrating the aspects of embodied carbon and structural reliability. These two parts are critical but sometimes it can be challenging to satisfy both criteria in design practice. This research used a probabilistic approach to link them together where its effectiveness was demonstrated. Thus, the RSIDO framework offers a way of designing reliable structures more sustainably. Furthermore, the adaptiveness of the RSIDO framework is highlighted by the newly formed RBDO problem, solved using the proposed AL-X-SVR-RBDO technique. Here, the surrogate model constructed in Stage I remains useful, as the probabilistic constraint related to the implicit limit state function does not change. However, the embodied carbon-related design constraint can lead to a shift in the feasible optimal region, requiring local enrichment of the surrogate model to improve accuracy in this newly focused area. Unlike traditional RBDO methods that require re-solving the entire problem, the high adaptiveness of the RSIDO method allows for targeted local enrichment, significantly improving efficiency. This framework also allows the method to handle a wide range of input uncertainties, including the distribution of the ECCs. This flexibility ensures the robustness of the method, making it applicable to constantly updating ECCs due to manufacturing advancements. In the future, the authors wish to extend the work for more sophisticated building systems considering multiple failure modes in accordance with design codes.

CRediT authorship contribution statement

Enyong Zhao: Writing – original draft, Visualization, Validation, Methodology, Investigation, Formal analysis, Conceptualization. **Qihan Wang:** Writing – review & editing, Software, Methodology, Conceptualization. **Mehrisadat Makki Alamdari:** Writing – review & editing, Supervision, Conceptualization. **Zhen Luo:** Writing – review & editing, Conceptualization. **Wei Gao:** Writing – review & editing, Supervision, Funding acquisition, Conceptualization.

Declaration of competing interest

The authors declare that they have no known competing financial interests or personal relationships that could have appeared to influence the work reported in this paper.

Acknowledgement

The work presented in this paper has been supported by Australian Research Council projects IH210100048, IH200100010, DP210101353, and DP240102559.

Appendix

For the overall readability and cohesion of the paper, some equations for the numerical investigation section are provided in this appendix.

The Stage III formulation of the investigated reinforced concrete beam is written as,

$$\begin{aligned}
&\min_{\mathbf{d}} \ A(\mu_w, \mu_h, \mu_d) \\
&s.t. \quad \Pr[g(\mathbf{X}, \mathbf{d}) = g(\mu_w, \mu_h, \mu_d, P, E_c, E_s) \le 0] \le \Phi\left(-\beta^T\right) \\
&\Pr[Q_{EC}(\mathbf{X}, \mathbf{d}) \le \widehat{Q}_{EC}] \le \Phi\left(-\beta_{EC}^T\right) \\
&g(\mathbf{d}, \mathbf{X}) = g(\mu_w, \mu_h, \mu_d, P, E_c, E_s) = 0.008 - \Delta(\mu_w, \mu_h, \mu_d, P, E_c, E_s) \\
&600 \ \text{mm} \le \mu_w \le 1000 \ \text{mm}, 800 \ \text{mm} \le \mu_h \le 1200 \ \text{mm}, 8 \ \text{mm} \le \mu_d \le 30 \ \text{mm} \\
&\beta^T = 3
\end{aligned} \tag{A1}$$

The Stage III formulation of the reinforced concrete slab is written as,

$$\begin{aligned}
&\min_{\boldsymbol{d}} \ m(\mu_d, \mu_h) \\
&s.t. \quad \Pr[g(\boldsymbol{d}, \boldsymbol{X}) = g(\mu_d, \mu_h, P, E_c, E_s, f_c, f_s, E_t) \le 0] \le \Phi\left(-\beta^T\right) \\
&\Pr[Q_{EC}(\boldsymbol{X}, \boldsymbol{d}) \le \widehat{Q}_{EC}] \le \Phi\left(-\beta_{EC}^T\right) \\
&g(\boldsymbol{d}, \boldsymbol{X}) = 0.01 - \Delta(\boldsymbol{d}, \boldsymbol{X}) \\
&8\text{mm} \le \mu_d \le 20\text{mm}, 50\text{mm} \le \mu_h \le 300\text{mm} \\
&\beta^T = 3
\end{aligned} \tag{A2}$$

In equations (A1) and (A2), the design objectives remain unchanged from the original RBDO problem in Stage I optimization. However, the total embodied carbon of the optimized structure $Q_{EC}(\boldsymbol{X}, \boldsymbol{d})$ is implemented into a new probabilistic constraint where the embodied carbon threshold $\widehat{Q}_{EC}$ is determined in Stage II, probabilistic uncertainty quantification of embodied carbon.

Data availability

Data will be made available on request.

References

[1] W. Pan, Y. Teng, A systematic investigation into the methodological variables of embodied carbon assessment of buildings, Renew. Sustain. Energy Rev. 141 (2021) 110840.
[2] F. Pomponi, A. Moncaster, Scrutinising embodied carbon in buildings: the next performance gap made manifest, Renew. Sustain. Energy Rev. 81 (2018) 2431–2442.
[3] Programme UNE, Global Status Report for Buildings and Construction, Global Alliance for Building and Construction, 2021.
[4] H. Gauch, C. Dunant, W. Hawkins, A.C. Serrenho, What really matters in multi-storey building design? A simultaneous sensitivity study of embodied carbon, construction cost, and operational energy, Appl. Energy 333 (2023) 120585.
[5] J. Hunt, C.A. Osorio-Sandoval, Assessing embodied carbon in structural models: a building information modelling-based approach, Buildings 13 (2023) 1679.
[6] V.J. Gan, J.C. Cheng, I.M. Lo, C.M. Chan, Developing a CO2-e accounting method for quantification and analysis of embodied carbon in high-rise buildings, J. Clean. Prod. 141 (2017) 825–836.
[7] M. Heydari, G. Heravi, A BIM-based framework for optimization and assessment of buildings' cost and carbon emissions, J. Build. Eng. 79 (2023) 107762.
[8] D. Fang, N. Brown, C. De Wolf, C. Mueller, Reducing embodied carbon in structural systems: a review of early-stage design strategies, J. Build. Eng. 76 (2023) 107054.
[9] M.S. Smith, D. Fang, C. Mueller, J. Carstensen, Reducing embodied carbon with material optimization in structural engineering practice: perceived barriers and opportunities, J. Build. Eng. (2024) 109943.
[10] S. Paneru, P. Ghimire, A. Kandel, S. Kafle, C. Rauch, Embodied residential building carbon emissions reduction in Nepal using linear optimization modeling, J. Build. Eng. 84 (2024) 108531.
[11] J. Li, T. Lützkendorf, M. Balouktsi, X. Bi, N. Alaux, T.P. Obrecht, et al., Identifying uncertainties in the whole life carbon assessment of buildings: sources, types, and potential actions, Build. Environ. (2023) 110779.
[12] A.M. Hasofer, N.C. Lind, Exact and invariant second-moment code format, J. Eng. Mech. Div. 100 (1974) 111–121.
[13] P. Hao, R. Ma, Y. Wang, S. Feng, B. Wang, G. Li, et al., An augmented step size adjustment method for the performance measure approach: toward general structural reliability-based design optimization, Struct. Saf. 80 (2019) 32–45.
[14] H.-M. Qian, H.-Z. Huang, Y.-F. Li, A novel single-loop procedure for time-variant reliability analysis based on Kriging model, Appl. Math. Model. 75 (2019) 735–748.
[15] P. Hao, H. Yang, H. Yang, Y. Zhang, Y. Wang, B. Wang, A sequential single-loop reliability optimization and confidence analysis method, Comput. Methods Appl. Mech. Eng. 399 (2022) 115400.
[16] X. Du, W. Chen, Sequential optimization and reliability assessment method for efficient probabilistic design, J. Mech. Des. 126 (2004) 225–233.
[17] J.P. Lima, Jr F. Evangelista, C.G. Soares, Hyperparameter-optimized multi-fidelity deep neural network model associated with subset simulation for structural reliability analysis, Reliab. Eng. Syst. Saf. 239 (2023) 109492.
[18] A.I. Oviedo, J.M. Londoño, J.F. Vargas, C. Zuluaga, A. Gómez, Modeling and optimization of concrete mixtures using machine learning estimators and genetic algorithms, Modelling 5 (2024) 642–658.
[19] M. Rezasefat, J.D. Hogan, Machine learning-assisted characterization of pore-induced variability in mechanical response of additively manufactured components, Modelling 5 (2023) 1–15.
[20] F. Hong, P. Wei, J. Fu, M. Beer, A sequential sampling-based Bayesian numerical method for reliability-based design optimization, Reliab. Eng. Syst. Saf. (2024) 109939.
[21] B. Echard, N. Gayton, M. Lemaire, AK-MCS: an active learning reliability method combining Kriging and Monte Carlo simulation, Struct. Saf. 33 (2011) 145–154.
[22] B. Sudret, Global sensitivity analysis using polynomial chaos expansions, Reliab. Eng. Syst. Saf. 93 (2008) 964–979.
[23] X. Zheng, W. Yao, X. Zhang, W. Qian, H. Zhang, Parameterized coefficient fine-tuning-based polynomial chaos expansion method for sphere-biconic reentry vehicle reliability analysis and design, Reliab. Eng. Syst. Saf. 240 (2023) 109568.
[24] M. Kolev, Predictive analysis of mechanical properties in Cu-Ti alloys: a comprehensive machine learning approach, Modelling 5 (2024) 901–910.
[25] G.G. Ali, I.H. El-adaway, M.O. Ahmed, R. Eissa, M.A. Nabi, T. Elbashbishy, et al., Forecasting future research trends in the construction engineering and management domain using machine learning and social network analysis, Modelling 5 (2024) 438–457.
[26] Q. Wang, D. Wu, G. Li, W. Gao, A virtual model architecture for engineering structures with Twin Extended Support Vector Regression (TX-SVR) method, Comput. Methods Appl. Mech. Eng. 386 (2021) 114121.
[27] Q. Wang, Q. Li, D. Wu, Y. Yu, F. Tin-Loi, J. Ma, et al., Machine learning aided static structural reliability analysis for functionally graded frame structures, Appl. Math. Model. 78 (2020) 792–815.
[28] R.M. Adnan, Z. Liang, S. Heddam, M. Zounemat-Kermani, O. Kisi, B. Li, Least square support vector machine and multivariate adaptive regression splines for streamflow prediction in mountainous basin using hydro-meteorological data as inputs, J. Hydrol. 586 (2020) 124371.
[29] B.J. Bichon, M.S. Eldred, L.P. Swiler, S. Mahadevan, J.M. McFarland, Efficient global reliability analysis for nonlinear implicit performance functions, AIAA J. 46 (2008) 2459–2468.

[30] Z. Sun, J. Wang, R. Li, C. Tong, LIF: a new Kriging based learning function and its application to structural reliability analysis, Reliab. Eng. Syst. Saf. 157 (2017) 152–165.
[31] X. Zhang, L. Wang, J.D. Sørensen, REIF: a novel active-learning function toward adaptive Kriging surrogate models for structural reliability analysis, Reliab. Eng. Syst. Saf. 185 (2019) 440–454.
[32] X. Zhang, Z. Lu, K. Cheng, Reliability index function approximation based on adaptive double-loop Kriging for reliability-based design optimization, Reliab. Eng. Syst. Saf. 216 (2021) 108020.
[33] E. Zhao, Q. Wang, M.M. Alamdari, W. Gao, Advanced virtual model assisted most probable point capturing method for engineering structures, Reliab. Eng. Syst. Saf. (2023) 109527.
[34] Q. Wang, Y. Feng, D. Wu, G. Li, Z. Liu, W. Gao, Polymorphic uncertainty quantification for engineering structures via a hyperplane modelling technique, Comput. Methods Appl. Mech. Eng. 398 (2022) 115250.
[35] Q. Wang, Y. Feng, D. Wu, C. Yang, Y. Yu, G. Li, et al., Polyphase uncertainty analysis through virtual modelling technique, Mech. Syst. Signal Process. 162 (2022) 108013.
[36] L. Du, R. Gao, P.N. Suganthan, D.Z. Wang, Bayesian optimization based dynamic ensemble for time series forecasting, Inf. Sci. 591 (2022) 155–175.
[37] M. Moustapha, S. Marelli, B. Sudret, Active learning for structural reliability: survey, general framework and benchmark, Struct. Saf. 96 (2022) 102174.
[38] B. Gaspar, A.P. Teixeira, C.G. Soares, Adaptive surrogate model with active refinement combining Kriging and a trust region method, Reliab. Eng. Syst. Saf. 165 (2017) 277–291.
[39] S.-Y. Huang, S.-H. Zhang, L.-L. Liu, A new active learning Kriging metamodel for structural system reliability analysis with multiple failure modes, Reliab. Eng. Syst. Saf. 228 (2022) 108761.
[40] P. Wu, Y. Feng, J. Pienaar, B. Xia, A review of benchmarking in carbon labelling schemes for building materials, J. Clean. Prod. 109 (2015) 108–117.
[41] C. Jones, G. Hammond, The inventory of carbon and energy ECE DB V3.0. 2019. https://circularecology.com/embodied-carbon-footprint-database.html, 2023. (Accessed 28 June 2024).
[42] SteelConstructioninfo, Embodied carbon coefficients used in the BCSA/SCI Carbon footprint tool for buildings. https://www.steelconstruction.info/images/6/6f/Embodied_carbon_coefficients_used_in_the_BCSA_carbon_footprint_tool_v2_16-07-14.pdf. (Accessed 28 June 2024).
[43] C. Barcelona, Steel beams and steel merchant bars Environmental Product Declaration. https://api.environdec.com/api/v1/EPDLibrary/Files/e3f50eec-82bc-4186-aabc-08db4497f421/Data, 2023. (Accessed 28 June 2024).
[44] E. steel, Non-alloy structural steel environmental product declaration. https://www.carescertification.com/files/approvals/1019/sustainability/1338.pdf, 2023. (Accessed 28 June 2024).
[45] BlueScope, Steel – welded beams and columns environmental product declaration. https://api.environdec.com/api/v1/EPDLibrary/Files/ff04419e-e321-468d-b640-3bb53cbad908/Data, 2020.
[46] I. Steel Dynamics, Fabricated structural steel sections environmental product declaration. https://pcr-epd.s3.us-east-2.amazonaws.com/469.EPD_for_Structural_FINAL_20191212.pdf. (Accessed 28 June 2024).
[47] B. Steel, THE FIRST CIRCULAR SUPPLY CHAIN, 2021. https://www.celsagroup.com/wp-content/uploads/pdf/BARNA_STEEL_datos%20celsa_infograf%C3%ADa.pdf. Accessed. (Accessed 28 June 2024).
[48] Aperam, Sustainability report 2021. https://www.aperam.com/sites/default/files/documents/2021_AperamMadeforLifeReport_Main.pdf, 2021. (Accessed 28 June 2024).
[49] A. Sostenible, Environmental product declaration reinforcing steel bar. https://api.environdec.com/api/v1/EPDLibrary/Files/08ed5a99-08e6-4bb1-a585-08dae89fe9e4/Data, 2022. (Accessed 28 June 2024).
[50] ABS, Sustainability report 2021. https://www.absacciai.com/wp-content/uploads/2022/05/ABS-Sustainability-Report_20_21.pdf, 2021. (Accessed 28 June 2024).
[51] Worldsteel, Sustainability indicators 2021 report. https://worldsteel.org/wp-content/uploads/Sustainability-Indicators-2021-Report.pdf, 2021. (Accessed 28 June 2024).
[52] InfraBuild, InfraBuild sustainability report 2021. https://www.infrabuild.com/resources/sustainability-resources/infrabuild-sustainability-report-2021/, 2021. (Accessed 28 June 2024).
[53] Liberty, Sustainability report 2021. http://libertysteelgroup.com/wp-content/uploads/2022/10/GFG_Sustainability-Report_2022_V11.pdf, 2021. (Accessed 28 June 2024).
[54] Iron MG, Sustainability report. https://www.mtgibsoniron.com.au/wp-content/uploads/2022/12/MGX-Sustainability-Report-2022.pdf, 2022. (Accessed 28 June 2024).
[55] BlueScope, Steel – hot rolled coil environmental product declaration. https://cdn.dcs.bluescope.com.au/download/environmental-product-declaration-hot-rolled-coil, 2020. (Accessed 28 June 2024).
[56] Association W. 2024.
[57] A. Hasanbeigi, M. Arens, J.C.R. Cardenas, L. Price, R. Triolo, Comparison of carbon dioxide emissions intensity of steel production in China, Germany, Mexico, and the United States, Resour. Conserv. Recycl. 113 (2016) 127–139.
[58] IEA, Emissions measurement and data collection for a net zero steel industry. https://www.iea.org/reports/iron-and-steel, 2023. (Accessed 28 June 2024).
[59] CO2CRC, Reduction of Greenhouse Gas Emissions in Steel Production, 2020.
[60] T. Wiedmann, S. Teh, M. Yu, ICM Database–Integrated Carbon Metrics Embodied Carbon Life Cycle Inventory Database, University of New South Wales, Kensington, Australia, 2019.
[61] V.J. Gan, C.M. Chan, K. Tse, I.M. Lo, J.C. Cheng, A comparative analysis of embodied carbon in high-rise buildings regarding different design parameters, J. Clean. Prod. 161 (2017) 663–675.
[62] G. Association, Carbon and energy impacts of steel products. https://galvanizing.org.uk/sustainable-construction/steel-is-sustainable/steel-embodied-carbon/, 2024. (Accessed 28 June 2024).
[63] W. Chen, S. Yang, X. Zhang, N.D. Jordan, J. Huang, Embodied energy and carbon emissions of building materials in China, Build. Environ. 207 (2022) 108434.
[64] I.Z. Bribián, A.V. Capilla, A.A. Usón, Life cycle assessment of building materials: comparative analysis of energy and environmental impacts and evaluation of the eco-efficiency improvement potential, Build. Environ. 46 (2011) 1133–1140.
[65] NSC, UK average embodied carbon of structural steel. https://www.newsteelconstruction.com/wp/wp-content/uploads/digi/NSCApr2021digi.pdf#page=25, 2021. (Accessed 28 June 2024).
[66] J. Xiao, C. Wang, T. Ding, A. Akbarnezhad, A recycled aggregate concrete high-rise building: structural performance and embodied carbon footprint, J. Clean. Prod. 199 (2018) 868–881.
[67] X. Zhang, X. Zhang, Sustainable design of reinforced concrete structural members using embodied carbon emission and cost optimization, J. Build. Eng. 44 (2021) 102940.
[68] P.E. Mergos, Seismic design of reinforced concrete frames for minimum embodied CO2 emissions, Energy Build. 162 (2018) 177–186.
[69] R. Kumanayake, H. Luo, N. Paulusz, Assessment of material related embodied carbon of an office building in Sri Lanka, Energy Build. 166 (2018) 250–257.
[70] W. Zhu, W. Feng, X. Li, Z. Zhang, Analysis of the embodied carbon dioxide in the building sector: a case of China, J. Clean. Prod. 269 (2020) 122438.